THE ASTROPHYSICAL JOURNAL, 456:717–737, 1996 January 10

ON THE INTERPRETATION OF THE ULTRAVIOLET SPECTRA OF SYMBIOTIC STARS AND RECURRENT NOVAE. II. THE 1985 OUTBURST OF RS OPHIUCHI

STEVEN N. SHORE
Department of Physics and Astronomy, Indiana University South Bend, 1700 Mishawaka Avenue, South Bend, IN 46634-7111
SCOTT J. KENYON
Harvard-Smithsonian Center for Astrophysics, 60 Garden Street, Cambridge, MA 02138
SUMNER STARRFIELD
Department of Physics and Astronomy, Arizona State University, Box 871504, Tempe, AZ 85287-1504
AND
G. SONNEBORN
Laboratory for Astronomy and Solar Physics, Code 681, Goddard Space Flight Center, Greenbelt, MD 20771
Received 1995 March 21; accepted 1995 June 16

ABSTRACT

We discuss the 1985 outburst of the symbiotic recurrent nova RS Oph using spectra obtained with the *International Ultraviolet Explorer* satellite and contemporaneous ground-based optical spectra. The low-resolution integrated fluxes show that a short-lived constant bolometric luminosity phase existed in the early outburst. If this reached the Eddington luminosity, it implies a minimum mass for the white dwarf of 1.2 $M_\odot$. This and the lack of evidence for eclipses in ultraviolet low-resolution spectra obtained in quiescence support the orbital solution of Dobrzycka & Kenyon (1994), in particular the low inclination of the system and the low mass, 0.5 $M_\odot$, of the red giant. The high-resolution optical and ultraviolet line profiles showed the development of two separate contributors. One was a broad-line component produced by emission from the high-velocity ejecta. The other was a narrow-line component produced in the portion of the red giant wind that was ionized by the UV pulse from the explosion and by radiation from the shock produced by the passage of the ejecta through the wind. The expanding Strömgren sphere had two effects. The strength of the line absorption from the overlying wind decreased against the ejecta and the ionized emitting gas, and the emission measure increased within the expanding H II region. We model these effects using the techniques developed in Shore & Aufdenberg (1993) to show how the column density of the cool material decreased with time. We show that the increased ionization of the wind accounts for changes in the absorption line components in the ultraviolet and use this decrease and the narrow emission-line ratios to determine the physical parameters for the line-forming region in the wind. From this, we derive the mass-loss rate for the red giant. In addition, we find evidence for a nitrogen overabundance in the wind using the time development of the N v 1240 Å doublet. The primary source for ionizing the red giant wind was radiation produced by the shocked ejecta as they traversed the stellar wind. The shock-generated emission also produced and powered the coronal species until about 100 days after ourburst at which time shock breakout occurred. The ionized wind subsequently recombined, although a hot source was still present on the white dwarf on the basis of continued visibility of the ultraviolet O III fluorescence lines and the IR He I 1.08 μm line. Finally, we discuss how many of the techniques developed in this study of a photoionizing pulse propagating into a dense environment can be applied to the analysis of active galactic nuclei.

Subject headings: binaries: symbiotic — galaxies: active — galaxies: nuclei — novae, cataclysmic variables — stars: individual (RS Ophiuchi)

1. INTRODUCTION

RS Ophiuchi is one of the few galactic recurrent novae (RNs) that is also a symbiotic binary system. Classical novae and some RNs are short-period systems (U Sco, V394 CrA, LMC 1990 No. 2, T Pyx), with orbital periods of order 1 day or less, and consist of a white dwarf and a compact secondary. In contrast, RS Oph and three others (T CrB, V745 Sco, V3890 Sgr) have very long orbital periods, several hundred days at least, and consist of a hot white dwarf and a red giant. The outburst is thought to be produced by a thermonuclear runaway on the white dwarf, initiated by mass accreted from the companion (Starrfield, Sparks, & Truran 1985; Starrfield, Sparks, & Shaviv 1988; Starrfield 1989). The criterion for a nova to be called recurrent is simply that it must have gone through multiple outbursts over the past 150 yr. By this criterion, RS Oph is one of the most active RNe, since it erupts about every 20 yr.

The 1985 outburst of RS Oph was one of the best studied outbursts of the century and it is the only RN whose entire outburst has been recorded across virtually the entire electromagnetic spectrum. Its development was observed from X-ray through centimeter radio wavelengths. RS Oph also has the special distinction of being the first nova outburst for which radio interferometric observations were able to resolve and map the ejecta in the early stages of the expansion.

This paper continues our exploration of the effects of absorption and emission lines from the red giant wind on the spectra of symbiotic stars and related systems. In Shore & Aufdenberg (1993, hereafter referred to as Paper I), we concentrated on the interpretation of ultraviolet spectra of quiescent

systems, mainly the classical symbiotics. We presented calculations of model spectra showing the effects of the myriad weak absorption lines from the iron group elements, the so-called "iron curtain," on the determination of wind properties. In this paper, we extend our study to the detailed examination of a highly time-dependent phenomenon, the outburst of one RN. In § 2, we briefly introduce the subclass of symbiotic RNs and the properties of the RS Oph binary system. After a presentation of the data and reduction methods in § 3, we discuss the UV properties of the system in quiescence and the evidence for permanent obscuration of the white dwarf by the intervening wind of the red giant. The observational description of the photometric and spectroscopic development of the 1985 outburst is presented in § 5. In § 6, we apply the methods developed in Paper I to the analysis of the red giant wind.

2. RECURRENT NOVAE AS A SUBCLASS OF NOVAE

The frequency of outbursts that characterize a RN is the result of the conditions in the accreted layer on the white dwarf. Theoretical models require that this star to be quite massive and very near the maximum allowable mass for a degenerate body, the Chandrasekhar limit, which is of order 1.4 $M_\odot$. Thus, they may be related to the ONeMg subclass of classical novae, which are also predicted to occur on massive white dwarfs (Politano et al. 1995).

RNs come in two distinct varieties depending on the evolutionary state of the companion (Shore, Livio, & van den Heuvel 1994a). The short-period systems, typified by the Galactic novae U Sco and V394 CrA and the extragalactic nova LMC 1990 No. 2, have compact companions that may be evolved, since helium overabundances or hydrogen deficiencies have been noted in both the ejecta and the accretion disk (Williams et al. 1981; Hanes 1985; Shore et al. 1991). The ejected mass is low, of order 10^{-7} to 10^{-6} $M_\odot$ and, unlike most slower classical novae, they never develop an optically thick "iron curtain" stage (see, e.g., Starrfield & Snijders 1989; Shore, Sonneborn, & Starrfield 1990; Hauschildt et al. 1992, 1994, 1995; Shore et al. 1994b). This stage occurs when the overlapping absorption-line spectrum, mainly due to singly ionized iron peak elements, is opaque and dominates the radiative transfer within the ejecta (Hauschildt et al. 1992; Shore et al. 1993, 1994b and references therein). Instead these RNs rapidly evolve into a stage characterized by optically thin emission lines.

In contrast, there is another class of RNs in which the secondary star is a red giant and the white dwarf orbits within its wind. They have long periods, of order years. The Galactic group consists of RS Oph, T CrB, V745 Sco, and V3890 Sgr (see, e.g., Gonzalez-Riestra 1992). There are no known extragalactic examples. During outburst they eject similarly low masses to the short-period systems at maximum velocities of order 2000–4000 km s^{-1}. Because of the dense circumstellar material around the white dwarf, the ionization pulse created by the nova should generate a time-dependent H II region that propagates outward in time and the shock generated by the ejecta should also emit hard ionizing radiation (Bode & Kahn 1985). Two major features of the spectra must therefore be modeled. The first is the broad emission from the optically thin ejecta of the nova itself. The second is the contribution from the wind. One of the most frequently observed phenomena, however, is the rapid appearance of narrow (less than 100 km s^{-1}) coronal and nebular emission lines within a few weeks of the outburst. These lines persist for several months, remaining long after the disappearance of the broad lines from the ejecta, and then slowly fade leaving a relatively low ionization emission-line spectrum that looks like a symbiotic star.

We note that there is a class of symbiotics that undergo much less energetic outbursts. However, the outbursts of the symbiotic RNs are more energetic than conventional symbiotic novae, like RR Tel, and much faster, so that their spectral evolution is far more time-dependent (Kenyon 1986; Mürset & Nussbaumer 1994). In the RN with red giant companions, the hard radiation pulse emitted by the outburst and the supersonic material ejecta traverse a dense environment. Since many of the spectral characteristics are similar to those observed in symbiotic novae, one expects that similar methods of analysis can be applied to the development of symbiotic RN spectra. It is perplexing that such similar systems should display such different behavior. One of the purposes of this paper is to illuminate the differences.

2.1. *RS Oph as a Binary System*

The orbital properties of RS Oph have been obtained by Dobrzycka & Kenyon (1994). Based on optical data, they found the following ephemeris for the inferior conjunction of the giant:

$$T(0) = 2444999.9(\pm 29^d.3) + 460^d(\pm 10^d)E \ .$$

They also reported that the eccentricity is either very small or zero. Assuming that the white dwarf is a 1.4 $M_\odot$ star, they obtained acceptable orbital solutions for only relatively low inclinations, $30° \leq i \leq 40°$. The upper limit comes from the lack of a strong reflection effect in this binary and the apparent absence of optical eclipses. The red giant mass they derived was quite low, of order 0.5 $M_\odot$. Dobrzycka & Kenyon also pointed out that the orbital properties are very similar to T CrB, another symbiotic RN with a higher inclination. T CrB was observed only at optical wavelengths during outburst, however, so any comparison between the two systems depends on their quiescent behavior. Paper I showed that the variations in the postoutburst ultraviolet spectrum of T CrB are likely due to orbital modulation as the hot remnant is seen through different column densities of intervening matter. Thus, by studying RS Oph in detail, we should also be able to gain insight into the outbursts of the T CrB system.

3. OBSERVATIONS AND REDUCTION METHODS

RS Oph was discovered in its fifth recorded outburst on 1985 January 26. Its visual brightness likely peaked on January 27 (JD 2,446,093) (Rosino & Iijima 1986). Its previous recorded outbursts were in 1898, 1933, 1958, and 1967 (Payne-Gaposchkin 1957; Bode 1986).

3.1. *Ultraviolet Observations*

Ultraviolet observations commenced with the *International Ultraviolet Explorer* satellite on February 2, about 6 days after optical maximum, and continued for the next 4 months. Early analyses of these spectra have been published by Cassatella et al. (1985), Snijders (1986, 1987), and Paper I.

The main data analyzed in this paper are all archival *IUE* spectra obtained during the 1985 outburst at high resolution (R = 10,000) using the large aperture (10 × 20 arcsec^2) taken with the Short Wavelength Primary (SWP, 1200–1930 Å) and Long Wavelength Primary (LWP, 2200–3300 Å) cameras. The journal of observations is given in Tables 1A and 1B. All spectra are available in the *IUE* archive through the NSSDC.

TABLE 1A

JOURNAL OF OBSERVATIONS: *IUE* HIGH-RESOLUTION SPECTRA, 1200–2000 Å

Spectrum	Date	Time (UT)	t_{exp} (s)	JD 2,440,000 +
SWP 25153.....	1985 Feb 2	20:26	1800	6099.351
SWP 25210.....	1985 Feb 10	4:29	2100	6106.687
SWP 25242.....	1985 Feb 14	11:48	5160	6110.992
SWP 25247.....	1985 Feb 15	3:29	2700	6111.645
SWP 25248.....	1985 Feb 15	4:40	1200	6111.694
SWP 25290.....	1985 Feb 21	12:16	3600	6118.011
SWP 25328.....	1985 Feb 27	1:2	3300	6123.543
SWP 25416.....	1985 Mar 10	6:51	6000	6134.785
SWP 25506.....	1985 Mar 23	8:51	7440	6147.869
SWP 25638.....	1985 Apr 9	5:34	9000	6164.732
SWP 25816.....	1985 Apr 30	6:40	10320	6185.778
SWP 25961.....	1985 May 17	4:23	17400	6202.683

TABLE 1B

JOURNAL OF OBSERVATIONS: *IUE* HIGH-RESOLUTION SPECTRA 2200–3300 Å

Spectrum	Date	Time (UT)	t_{exp} (s)	JD (2,440,000 +)
LWP 5363.....	1985 Feb 14	12:43	720	6111.030
LWP 5370.....	1985 Feb 15	4:29	420	6111.687
LWP 5429.....	1985 Feb 27	1:42	660	6123.571
LWP 5479.....	1985 Mar 10	0:0	1380	6134.500
LWP 5585.....	1985 Mar 23	7:52	1800	6147.838
LWP 5705.....	1985 Apr 9	3:57	1800	6164.665
LWP 5707.....	1985 Apr 9	8:10	4320	6164.840
LWP 5866.....	1985 Apr 30	4:55	1800	6185.705

The data were extracted using standard routines available through the *IUE* Data Analysis Facility at Goddard Space Flight Center (IUEDAC Staff 1994). We also use low-resolution ($R = 300$) SWP spectra to study the photometric variations of the system (see below, § 5.2).

3.2. *Optical Spectra*

All the optical spectra analyzed here were obtained in 1985 by R. E. McCrosky using the echelle spectrograph and intensified Reticon detector on the 1.5 m telescope of Oak Ridge Observatory (see Latham 1985). These data have a resolution of 12 km s^{-1} in 40–60 Å bandpasses centered on strong emission features at λ4686 (He II), λ4861 (Hβ), λ5303 (Fe II, [Fe XIV]), λ6087 ([Fe VII]), λ6563 (Hα), and λ6830 (Raman scattered O VI). Each observation consisted of a 90 s Th-Ar comparison scan before and after a 10–20 minute exposure of RS Oph. The strong comparison lines (~30) were fitted with a fifth-order polynomial having typical residuals of 0.01 Å (~0.5 km s^{-1}). The λ6830 order had only 15 useful comparison lines for a wavelength solution, so the uncertainty in the wavelength calibration was ~0.03 Å for this order. The λ6830 feature is significantly broader than other emission lines in RS Oph (see below); larger errors in the velocity scale are not important. Finally, each scan was divided by normalized observations of a tungsten lamp to remove the echelle blaze and to correct for fixed pattern noise and pixel-to-pixel variations within the Reticon. Table 4 presents a journal of observations in the form of the He II 4686 Å fluxes.

In a future publication (Kenyon et al. 1995) we will provide a multiwavelength atlas of high-resolution line profiles from the 1985 outburst. Here we discuss only the specific aspects of the optical spectra that relate to physical quantities derived from the ultraviolet observations.

4. LOW-RESOLUTION SPECTRA OUTSIDE OF OUTBURST AND ORBITAL MODULATION

The high-resolution UV data obtained during the outburst were all taken during a single orbit of RS Oph during the phase interval 0.39 (SWP 25153) to 0.62 (SWP 25961), when the white dwarf was at inferior conjunction. Thus, these data provide no information about possible phase-dependent effects. In order to investigate the effects of possible orbital modulation on the ultraviolet spectra, we used archival low-resolution data taken outside the outburst period. These spectra are listed in Table 2, along with their orbital phases and integrated SWP fluxes, and shown in Figure 1. They are generally weakly exposed, but they span the several years before outburst and nearly 8 yr afterward.

These data support the conclusion by Dobrzycka & Kenyon (1994) that there are no eclipses, although the later well-exposed spectra contain evidence for line absorption by the red giant wind in the spectral region between 1500 Å and 1700 Å. The only emission line consistently present in the low-resolution spectra is N III] 1750 Å which is especially strong in the first spectrum (SWP 6608). Curiously, the 1982 spectrum, SWP 18387, is much brighter than any of the others and was obtained during an optical brightening. Such brightenings seem to occur regularly (Dobrzycka & Kenyon 1994), and it is not clear whether they have anything to do with the major outbursts. The brightenings do not seem to be due to changes in the amount of intervening wind material because the ultraviolet spectra show no substantial changes during these times.

TABLE 2

JOURNAL OF OBSERVATIONS: *IUE* LOW-RESOLUTION QUIESCENT SPECTRA

Spectrum	Date	Time (UT)	Phase	t_{exp} (s)	Integrated Flux	JD (2,440,000 +)
SWP 6608	1979 Sep 22	22:18	0.13	1920	3.62E−12	4139.436
SWP 13954.....	1981 May 10	10:38	0.42	14400	3.72E−12	4734.938
SWP 18387.....	1982 Oct 25	9:45	0.60	3600	1.60E−11	5267.906
SWP 26882.....	1985 Oct 6	16:35	0.92	3600	4.31E−12	6345.264
SWP 28825.....	1986 Aug 4	0:0	0.58	6960	4.68E−12	6646.605
SWP 30423.....	1987 Mar 2	9:19	0.04	9420	5.99E−12	6856.834
SWP 33453.....	1988 May 5	5:17	0.97	10800	4.02E−12	7286.658
SWP 40979.....	1991 Mar 2	14:14	0.23	20400	5.46E−12	8317.975
SWP 42293.....	1991 Aug 20	7:23	0.58	16500	7.70E−12	8488.712

NOTE.—All fluxes are quoted as ergs s^{-1} cm^{-2}.

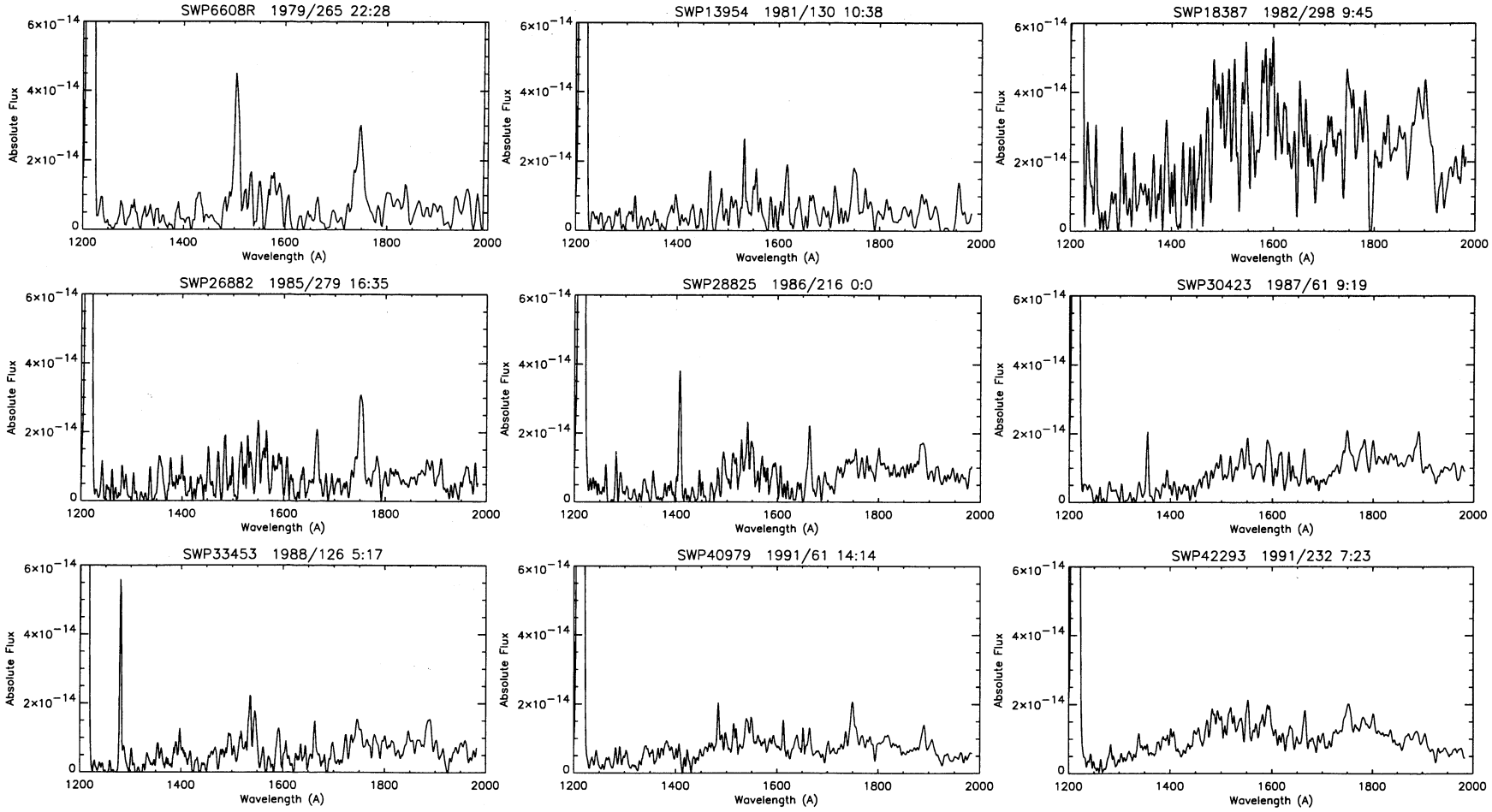

FIG. 1.—Atlas of low-resolution SWP spectra taken in quiescence. Note that the N III] 1750 line is the only clearly detected emission. The region between 1500 and 1700 Å is dominated by iron peak absorption lines from the red giant wind. Spectrum SWP 18387 is the anomalous brightening referred to in the text.

5. THE DEVELOPMENT OF THE 1985 OUTBURST

5.1. *Taxonomy of the Outburst*

Rosino (1986) provides a breakdown of the development of the optical spectrum. During the first 2 days following visual maximum, broad emission lines of H I, He I, and Fe II are observed with narrow absorption components ($v \approx 40$–60 km s^{-1}) and broad P Cygni troughs ($v_{max} \approx -2700$ to -3900 km s^{-1}). As we will discuss, the high-velocity components are formed in the ejected matter from the explosion and the narrow absorption lines arise in the cool wind material superposed between the white dwarf and ejecta and the observer. From days 2 to 15, He II 4686 Å, [N II], [O I], [O III], [Ne III], [S II], and [Fe X] 6374 Å appear. The He II and N III 4630 Å lines strengthen through day 30. The period from days 30 through 50 is marked by the maximum strength of the He II 4686 Å line. The coronal line phase lasts from about days 51 to 130, and is marked by the appearance of [Ar X], [Fe X], [Fe XI], [Fe XIV] and the peaking of the lower ionization nebular emission lines, the profiles of which become more diffuse with time. Finally, the interval from day 131 to day 200 is marked by the fading of the coronal lines and the weakening of the He II and Fe II lines.

We divide the ultraviolet development into similar phases. The first was the broad-line phase when the material ejected at high velocities dominated the emission. This lasted until about day 60. The second phase began when narrow emission from the newly ionized red giant wind appeared and then dominated the spectrum. This was still during the optical coronal line stage. The decline of the ultraviolet coronal lines followed the time when the narrow lines and also marked the onset of recombination, a phase we will refer to as the "breakout" stage (see below).

5.2. *Photometric Variations*

Simultaneous optical photometry of the outburst was obtained during each SWP and LWP exposure using the Fine Error Sensor (FES) on the *IUE* satellite. This instrument has a broad visual spectral response, and it provides a useful contemporaneous record of the optical fluxes. The counts were converted to V magnitudes using the algorithm described by Loomis (1994 and references therein); they are given in Table 3, corrected for $E(B-V) = 0.75$ mag (Snijders 1986; Evans et al. 1988). Accompanying most high-resolution *IUE* observations, low-resolution ($R = 300$) SWP spectra were obtained with the large aperture. There were only three well-exposed, large-aperture, low-resolution LWP spectra. The integrated ultraviolet fluxes are also given in Table 3. In Figure 2, we show the multiwavelength photometric variations of RS Oph, including the *EXOSAT* X-ray counts, and the ultraviolet, visual, infrared, and radio fluxes.

The resulting integrated flux can thus be derived for only three dates. On JD 2,446,106 and JD 2,446,117, it was 4.86×10^{-7} and 4.58×10^{-7} ergs s^{-1} cm^{-2}, respectively. By JD 2,446,198, it had fallen to 1.98×10^{-8} ergs s^{-1} cm^{-2}. Using the distance of 1.6 kpc from Hjellming et al. (1986) and Snijders (1986), the bolometric luminosity at peak corresponds to $3.7 \times 10^4\ L_\odot$, the Eddington luminosity for a $1.2\ M_\odot$ white dwarf assuming solar composition and electron scattering opacity. We emphasize that this is a lower limit because we have not been able to include the ultraviolet flux below 1200 Å. Thus, the mass of the white dwarf may be close to the Chandrasekhar limit and it is similar to the value suggested by Starrfield et al. (1985) (see also Starrfield et al. 1988) for the RN U Sco. The low ejecta mass (see below) and the speed of the optical and UV light variations during the broad-line phase support this suggestion. A high-mass white dwarf is consistent with the orbital solution of Dobryzcka & Kenyon (1994).

5.3. *Broad-Line Phase: The Nova Ejecta*

The atlas of high-resolution spectra is shown in Figure 3, binned to $\Delta\lambda = 0.5$ Å, and the integrated line fluxes from these binned spectra are given in Tables 4, 5, and 6. The integrated line fluxes are plotted in Figures 4*a* and 4*b*. The first SWP spectrum, taken on JD 2,446,099, was dominated by two strong, broad emission lines, O I + Si III 1300 Å and N III] 1750 Å. There were no other emission lines present in the spectrum at this time, but a strong absorption-line spectrum from the red giant wind was clearly present throughout the 1200–2000 Å region (see Fig. 3). The O I and N III] lines were very broad, showing FWZI of 7000 km s^{-1} and FWHM of about 4000 km s^{-1}. Superposed on these emissions were narrow absorption

TABLE 3

INTEGRATED LOW-RESOLUTION FLUXES

JD (2,440,000 +)	F(SWP)[a]	F(LWP)[b]	F(*V*)[c]
6099.28	4.46E−07	...	7.14E−08
6106.59	2.98E−07	1.53E−07	3.46E−08
6110.92	2.89E−07	...	2.54E−08
6117.92	3.22E−07	1.19E−07	1.73E−08
6123.50	3.82E−07	...	1.16E−08
6134.50	2.86E−07	...	6.86E−09
6134.82	2.87E−07	...	6.84E−09
6147.73	2.03E−07	...	5.52E−09
6153.59	1.74E−07	...	4.39E−09
6164.57	1.11E−07	...	3.32E−09
6185.60	2.86E−08	...	1.12E−09
6198.01	1.49E−08	4.13E−09	8.38E−10

NOTES.—All fluxes are dereddened using $E(B-V) = 0.75$ and are in units of ergs s^{-1} cm^{-2}.

[a] Integrated 1200–2000 Å flux.

[b] Integrated 2200–3400 Å flux.

[c] Converted from FES counts (see text).

TABLE 4

INTEGRATED He II 4686 Å FLUXES DURING OUTBURST

JD (2,440,000P+)	*F*(He II 4686 Å)
6112.75.....	4.35E−10
6117.00.....	3.59E−10
6124.75.....	3.62E−10
6127.75.....	5.78E−10
6132.00.....	5.66E−10
6136.00.....	4.77E−10
6141.00.....	2.08E−10
6158.75.....	1.28E−10
6163.00.....	1.21E−10
6189.75.....	7.46E−11
6200.75.....	1.90E−11

NOTE.—Spectrophotometric values for line fluxes have been measured on 1985 Mar 1 (JD 6204.48): F(He II 4686) = 1.9×10^{-11}; $F(H\beta\ 4861) = 4.1 \times 10^{-11}$; F([Fe XIV] 5303 + Fe II 5316) = 1.0×10^{-11}. Fluxes are in units of ergs s^{-1} cm^{-2}.

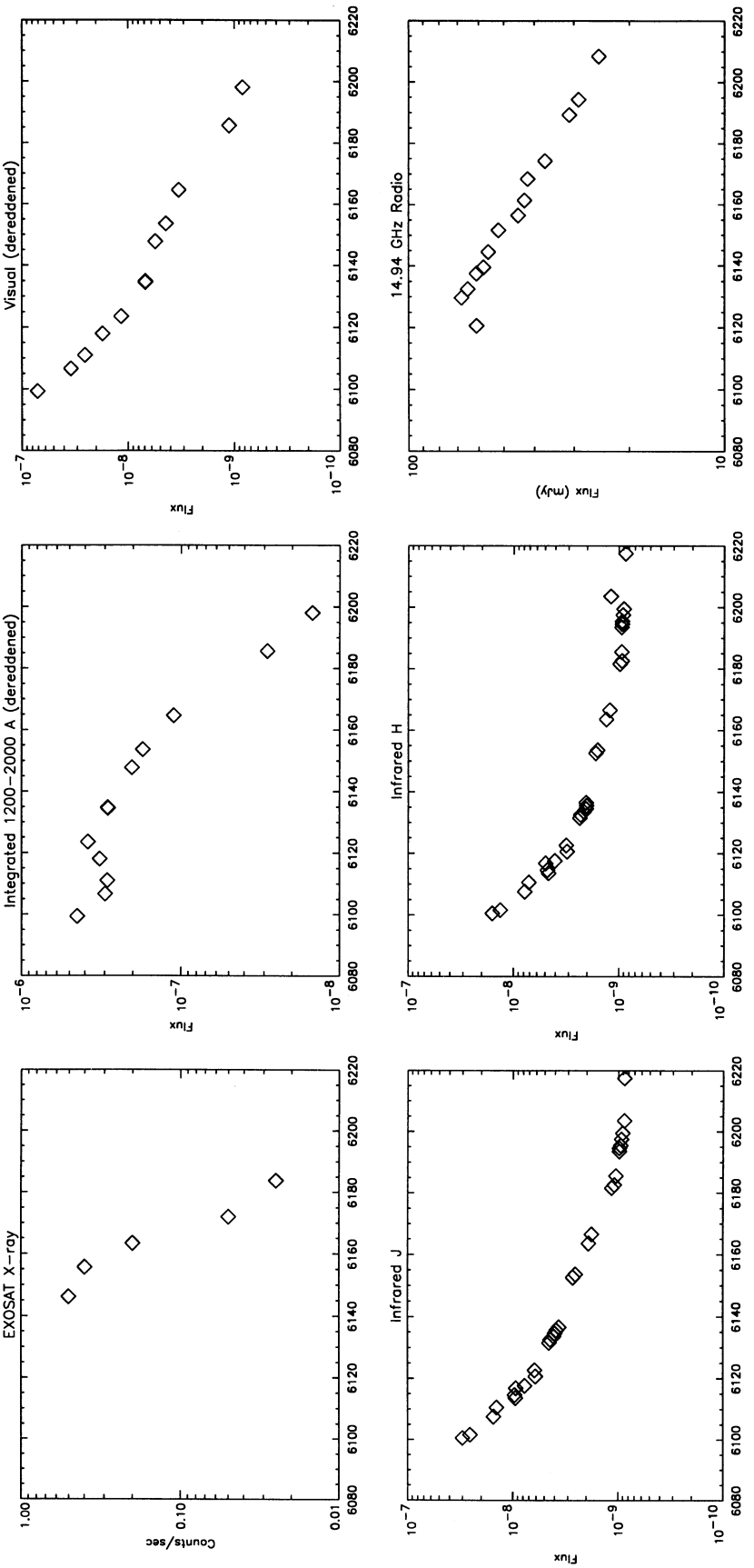

FIG. 2.—Comparative photometric variations of RS Oph during the 1985 outburst curve. The curves show the *EXOSAT* counting rates (Mason et al. 1986); integrated 1200–2000 Å light curve; FES visual fluxes; infrared fluxes (Evans et al. 1988); and radio fluxes (Hjellming et al. 1985). Units for all but the X-ray fluxes are ergs s^{-1} cm^{-2}. No extinction corrections have been applied.

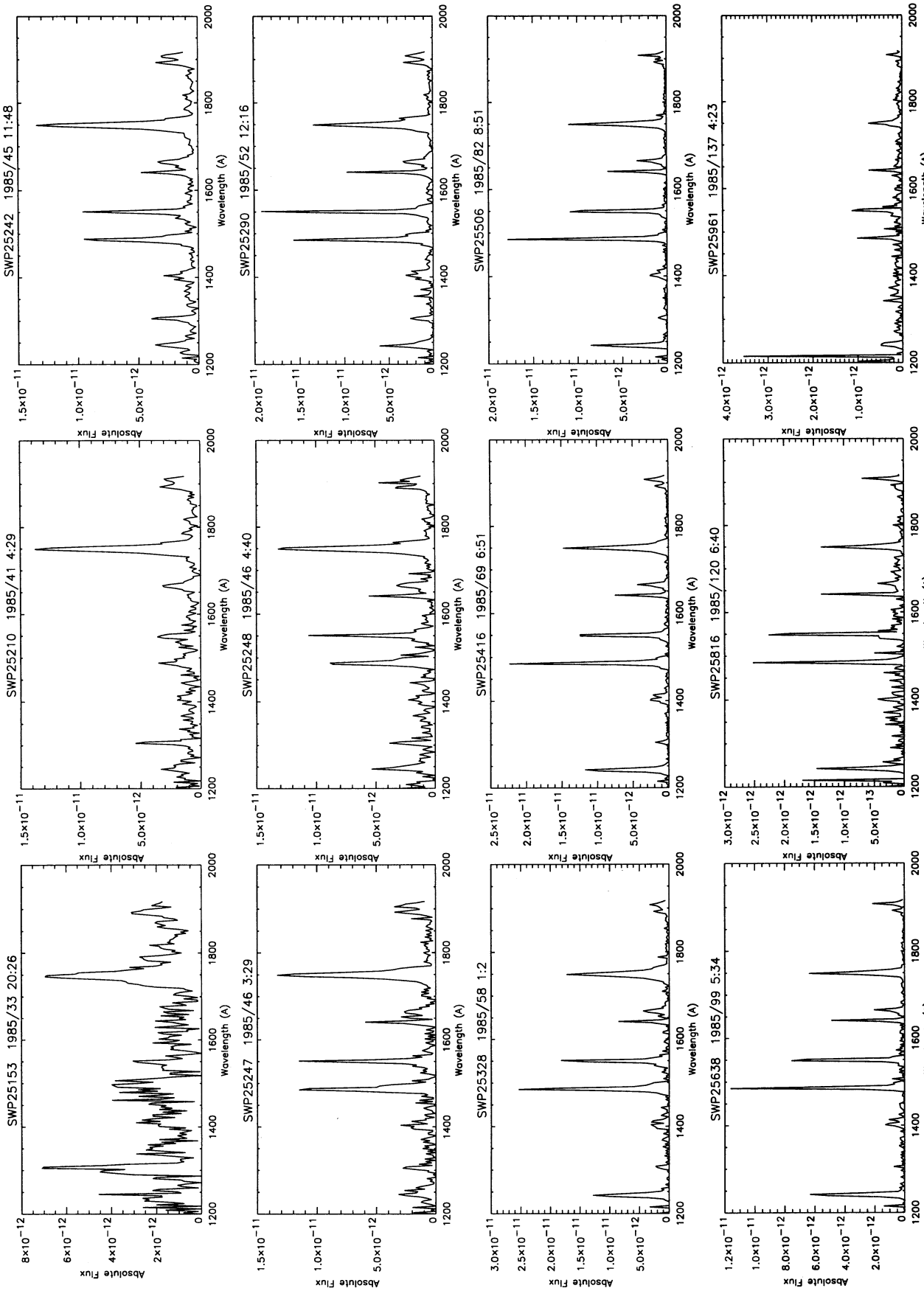

FIG. 3.—Atlas of high-resolution 1200–3300 Å *IUE* spectra binned to 0.5 Å resolution showing the development of the emission lines throughout the outburst. Units are ergs s^{-1} cm^{-2} $Å^{-1}$

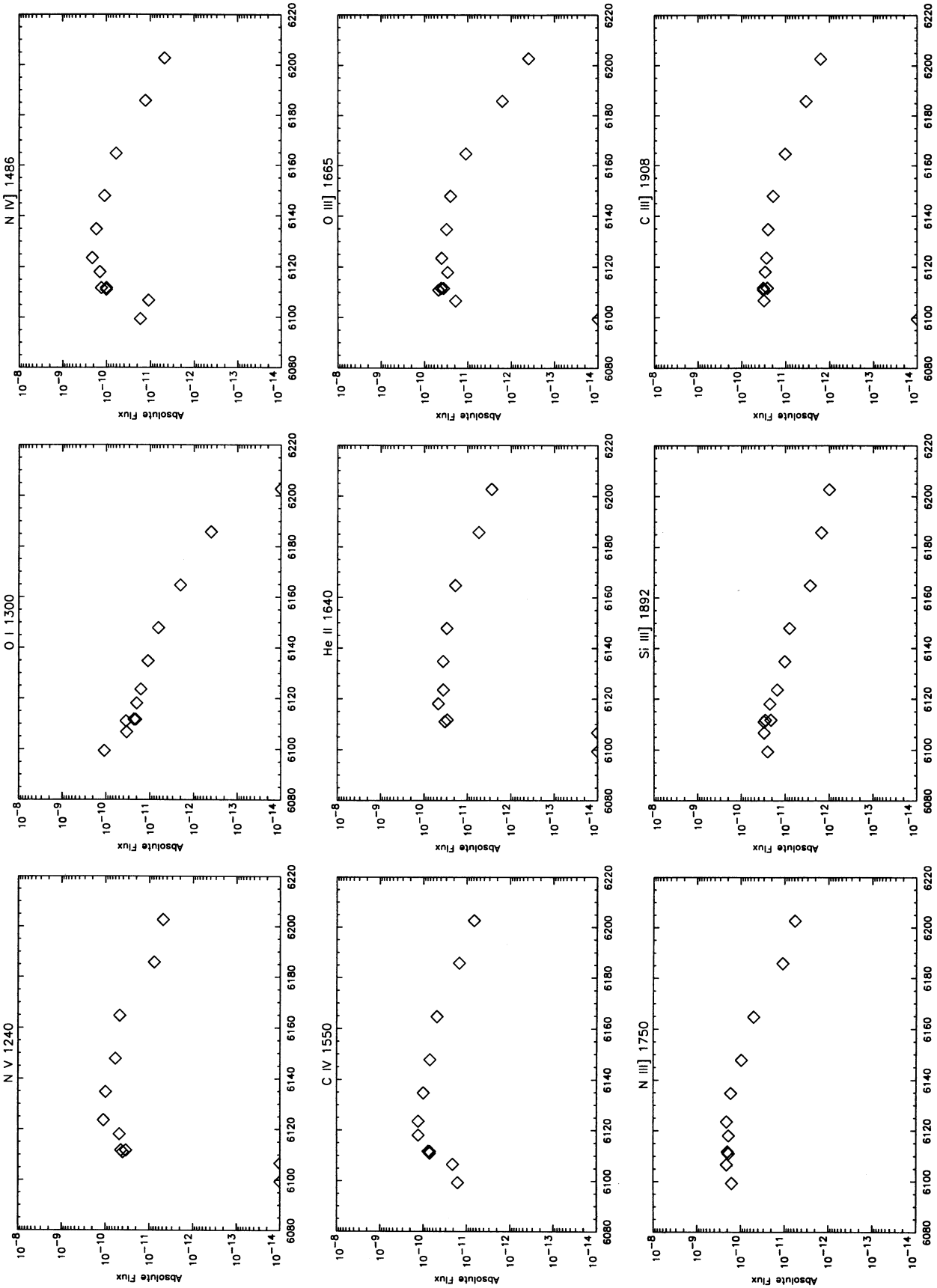

FIG. 4.—Variation of the integrated emission line fluxes in the ultraviolet through the outburst. Units are ergs s^{-1} cm^{-2}.

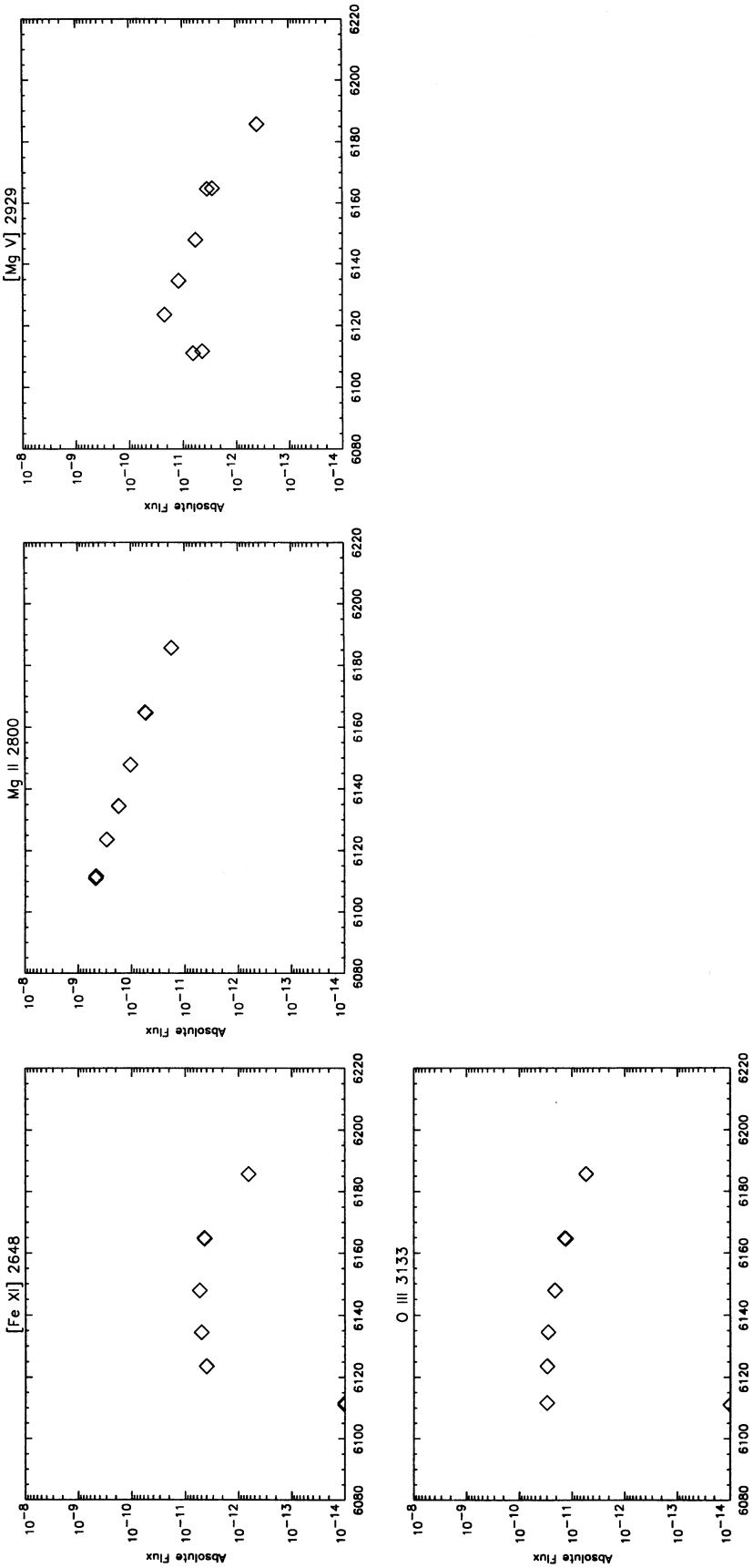

FIG. 4.—*Continued*

TABLE 5

INTEGRATED SWP LINE FLUXES: 0.5 Å RESOLUTION

SWP	N v 1240	O i 1300	N iv] 1486	C iv 1550	He ii 1640	O iii] 1665	N iii] 1750	Si iii] 1892	C iii] 1908
25153.....	...	1.08E−10	1.70E−11	1.61E−11	...	...	1.57E−10	2.48E−11	...
25210.....	...	3.35E−11	1.08E−11	2.07E−11	...	1.89E−11	2.06E−10	3.02E−11	3.05E−11
25242.....	3.97E−11	3.52E−11	1.04E−10	7.06E−11	3.26E−11	4.66E−11	1.93E−10	3.00E−11	3.17E−11
25247.....	3.40E−11	2.13E−11	1.27E−10	7.10E−11	2.90E−11	3.60E−11	2.01E−10	2.79E−11	3.17E−11
25248.....	4.43E−11	2.31E−11	1.00E−10	7.66E−11	2.92E−11	4.14E−11	1.95E−10	2.13E−11	2.56E−11
25290.....	4.78E−11	1.97E−11	1.43E−10	1.30E−10	4.67E−11	2.87E−11	1.84E−10	2.21E−11	2.85E−11
25361.....	1.13E−10	1.57E−11	2.08E−10	1.2E−10	3.65E−11	3.99E−11	2.10E−10	1.48E−11	2.65E−11
25416.....	9.85E−11	1.07E−11	1.67E−10	9.87E−11	3.57E−11	3.11E−11	1.66E−10	1.02E−11	2.48E−11
25506.....	5.92E−11	6.37E−12	1.08E−10	7.04E−11	3.00E−11	2.51E−11	9.73E−11	7.86E−12	1.88E−11
25638.....	4.68E−11	<2.1E−12	6.01E−11	4.86E−11	1.89E−11	1.13E−11	5.08E−11	2.74E−12	1.02E−11
25816.....	7.80E−12	<4.0E−13	1.28E−11	1.49E−11	5.49E−12	1.56E−12	1.06E−11	1.50E−12	3.35E−12
25961.....	4.92E−12	...	4.78E−12	6.83E−12	2.69E−12	<4.0E−13	5.81E−12	1.00E−12	1.60E−12

NOTE.—All fluxes are in units of ergs s^{-1} cm^{-2}.

lines arising from the red giant wind. The next set of spectra, taken about a week later, showed that considerable evolution has occurred. The ionization of the ejecta had increased substantially and both the Si IV 1400 Å doublet and weak C IV 1550 Å doublet emissions were present. In the LWP range, only Mg II 2800 Å was in emission. This was probably true as well during the earlier stages of the outburst, but we do not have spectra from before JD 2,446,106.

The broad lines gradually narrowed, decreasing to a FWZI of less than 3000 km s^{-1} by JD 2,446,202. This is usual in nova spectra and caused by the distribution of velocity in the matter at the moment of ejection: the fastest moving gas travels farthest in a given time interval (see e.g., Starrfield et al. 1974; Shore et al. 1993, and references therein). As the density of the shell decreases, so does the emissivity at any velocity with the consequent narrowing of the lines. During the line-narrowing stage, the ionization of the expanding gas increases because the hot central source continues to illuminate and ionize the ejecta. This clearly happened in RS Oph. These features and their evolution confirm that the ejection occurred in an explosion and not by an episodic mass transfer event, as suggested by Livio et al. (1986). In addition, the ionization pulse produced during the earliest stage of the explosion continued to propagate through the red giant wind.

Broad, high-ionization lines, such as He II 1640, N V 1240, and N IV] 1486, and lower ionization lines such as Si III] 1892, C III] 1908, and O III] 1665, increased in strength until JD 2,446,147. With the exception of O I 1300 Å, N III] 1750 Å, and Mg II 2800 Å, which decreased monotonically from the first observation, all of the emission lines peaked simultaneously on JD 2,446,147. This behavior is shown in Figure 4. Note that these integrated line fluxes include both the broad and narrow emission components. As we will discuss presently, the profiles were dominated by the broad-line phase in the initial expansion.

The ratio of the integrated line fluxes for Si III] 1892 Å to C III] 1910 Å, which measures the electron density (Nussbaumer & Stencel 1989), steadily decreased from an initial value of 1.0 on JD 2,446,106 to a minimum of 0.3 on JD 2,446,164. This means that the density in the emitting gas had decreased. However, the ratio again began to rise thereafter, reaching 0.6 by JD 2,446,202. This evolution in the ratio indicates that the density of the gas contributing to the integrated fluxes decreased to 10^9 cm^{-3} and then increased to about 10^{10} cm^{-3}. We interpret this spectral evolution as being due to the emission from the high-velocity ejecta decreasing in strength due to expansion while the ionized low-density regions of the red giant wind were beginning to dominate the line profiles. Subsequently, as the wind recombined, progressively denser parts of the wind were emitting in these ions. The change in the line ratio occurred at the time when the broad lines peaked and the thermal radio emission peaked at the same time (Spoelstra et al. 1987; Taylor et al. 1989). It was also at this time that the X-ray emission entered its rapid decline (Mason et al. 1986; see also Itoh & Hachisu 1990). The broad-line phase ended quickly thereafter. This means that the ejecta were no longer contributing to the formation of the emission-line profiles. We refer to this as *breakout* in analogy to the stage in a thermonuclear explosion when the shock emerges from the environmental fireball.

5.4. *Narrow Emission Phase: Expanding Strömgren Sphere*

The narrow emission-line phase marked the gradual emergence in the spectrum of lines from the expanding Strömgren

TABLE 6

INTEGRATED LWP LINE FLUXES: 0.5 Å RESOLUTION

LWP	[Fe XI] 2648	He II 2733	Mg II 2800	[Mg V] 2929	λ2936	O III 3023	O III 3133
5363.....	...	...	4.72E−10	6.45E−12	9.76E−12	<4.3E−13	4.33E−12
5370.....	...	<3.0E−12	4.63E−10	4.36E−11	...	<1.2E−12	2.98E−11
5429.....	4.02E−12	2.84E−12	2.92E−10	2.20E−11	3.88E−11	5.89E−12	2.95E−11
5479.....	4.99E−12	2.02E−12	1.75E−10	1.19E−11	2.51E−11	2.10E−12	2.83E−11
5585.....	5.38E−12	1.21E−12	1.05E−10	5.77E−12	1.29E−11	8.46E−13	2.10E−11
5705.....	4.31E−12	1.25E−12	5.36E−11	3.48E−12	7.02E−12	5.06E−13	1.39E−11
5707.....	4.46E−12	1.84E−12	5.57E−11	2.78E−12	6.97E−12	5.86E−13	1.38E−11
5866.....	6.50E−13	5.70E−13	1.75E−11	4.00E−13	1.91E−12	<1.9E−13	5.44E−12

NOTE.—All fluxes are in units of ergs s^{-1} cm^{-2}.

sphere formed by the short-duration ultraviolet pulse from the explosion propagating into the red giant wind. This occurred about 60 days into the outburst. The line formation is far from equilibrium since the source was an initial UV pulse, and since the wind has a large density gradient. Thus we expect that different portions of the wind will contribute to different parts of the line profile. It should be emphasized that the narrow emission lines could not have originated in the ejecta. Their appearance coincided with the disappearance of the narrow absorption features on C IV and He II, and their velocity width is more typical of those observed for red giant winds (they are likely unresolved in the high-resolution *IUE* spectra, $\lesssim 30$ km s^{-1}).

The high-resolution C IV 1550 Å doublet profiles can be used to trace the changing column density of the cool red giant wind as the ionization pulse propagates through it (see also Paper I). The ratio of the narrow emission-line components [F(1548 Å)/F(1550 Å)] is shown in Figure 5 and the data are listed in Table 8. In the initial spectrum showing the narrow components (SWP 25248), only the 1550 Å line is visible. The 1548 Å component gradually dominated the 1550 Å component, and the line ratio gradually increased to about 2 by the end of the outburst spectral sequence. This is due to a decrease in the selective absorption by cool gas in the overlying giant wind as discussed in Paper I. This will be detailed further in § 6.3.

There is additional evidence for the absorption of the C IV emission components by the cool gas in the form of fluorescent emission by Fe II. Meier et al. (1994, and references therein) discussed how C IV emission can power iron fluorescence in the ambient gas by populating very elevated levels in Fe II. This accounts for the flux redistribution from the absorption. Singly ionized iron fluorescence transitions were detectable on one spectrum, LWP 5707. This was the longest exposure of the series, and the one with the highest S/N ratio. Consequently, it is possible that the Fe II emission lines were present before this stage but too weakly exposed to be detected. The transitions arise from C IV 1550 Å pumping from the Fe II $a\,^4F_{9/2}$ state to the $y\,^4H^o_{11/2}$ state, with subsequent decay through the $a\,^4G$ and $b\,^2H$ states, as noted for RR Tel and V1016 Cyg by Johansson (1983). In particular, the strongest Fe II lines were detected at 2458.78, 2481.05, and 2492.34 Å (laboratory wavelengths). For these spectral regions, we show a comparison between a deeply exposed RR Tel spectrum, LWP 25954, and LWP 5707 in Figure 6. This LWP spectrum was obtained well into the decline phase of the C IV resonance lines, and it is probable that the fluorescent transitions were even stronger earlier. In Paper I, we discussed the pumping of the upper state of the 1641 Å transition by resonance absorption from O I 1302 Å, which implied that there was a large column density of neutral wind material absorbing O I and Si III emission from the embedded ejecta and redistributing it in the forbidden line.

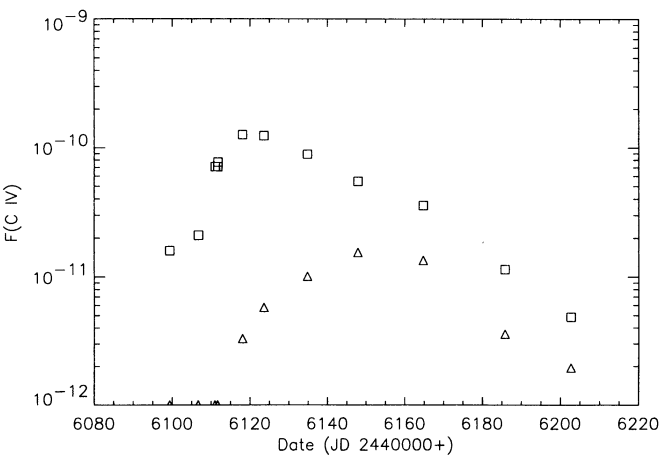

FIG. 5.—Variation of the narrow (*triangles*) to broad (*squares*) line fluxes for the C IV 1550 Å doublet.

Optical Fe II fluorescence was detected almost immediately during the outburst, as early as JD 2,446,101. Strong narrow emission appeared at 5316 Å, which is a transition connected with the ^4G state (Fawcett 1988). The line developed the same high-velocity feature detected on all of the other narrow components after JD 2,446,125. This feature disappeared by JD 2,446,227, after the end of the *IUE* spectral sequence. Interestingly, the low-velocity component gradually broadened between JD 2,446,189 and JD 2,446,227, perhaps indicating that a larger velocity gradient was sampled by recombinations in the last spectra.

The optical 6830 Å emission feature, attributed to Raman scattering by O VI (Schmid 1989), remained broad throughout the outburst. Its intensity followed the decrease in the UV continuum, but the line width declined relatively little throughout the outburst. This finding agrees with its identification as a Raman line. Its presence indicates that a hot EUVE emitting source was present through much of the outburst.

The emission lines from a number of coronal species appeared after the start of the narrow-line phase, in particular [Mg V] 2783 Å and [Fe XI] 1467 Å and 2648 Å. The line flux variations are shown in Figure 4 and in Table 6. The [Fe XI] 2648 Å line was quite strong. There was weak emission from [Fe XII] 1349 Å, 2405 Å, and 2565 Å. However, we note that a search of the 1200–3300 Å region failed to detect the [Fe XII] 1242.00 Å line in any spectra, and [Fe XII] 1349.40, 2405.68, and 2565.93 Å were only very weak if they were present at all. The [Fe XIV] 5302.86 Å coronal line displayed virtually the same profile as the [Fe XI] 2648 Å line throughout the outburst, appearing on JD 2,446,125 and disappearing by JD 2,446,200, coincident with the rapid fading of the [Fe XI] ultraviolet line. This shows that the source of ionization had high radiation temperatures in excess of 3×10^6 K. Although not visible in the high-resolution data, [Mg V] 1815 Å was detected in low-resolution spectra, but was always very weak. Two well-exposed, large-aperture, low-resolution spectra, SWP 25504 and SWP 25636, show this line. It is clearly absent in the low-resolution spectrum SWP 25920, taken at the same time as the last high-resolution spectrum in this data set (SWP 25961). Thus the [Mg V] decline followed that of the other coronal emission lines.

Snijders (1986) attributed the appearance of coronal lines to their formation in a postshocked gas produced by the ejecta. If this were correct, the emission lines should have been very broad, and they are in fact quite narrow. There is, however, another interpretation. The increased ionization of the low-density gas in the periphery of the red giant wind is produced by the Strömgren sphere generated by the initial UV pulse and continued ionization by radiation from the wind-shocked ejecta. Support for this interpretation comes from the fact that the coronal lines were always narrow, and their widths were consistent with other narrow lines arising from the red giant wind.

5.5. *Shock Breakout*

Although there is no "edge" to the wind, we define breakout as that stage when the X-ray emissivity from the shock is no

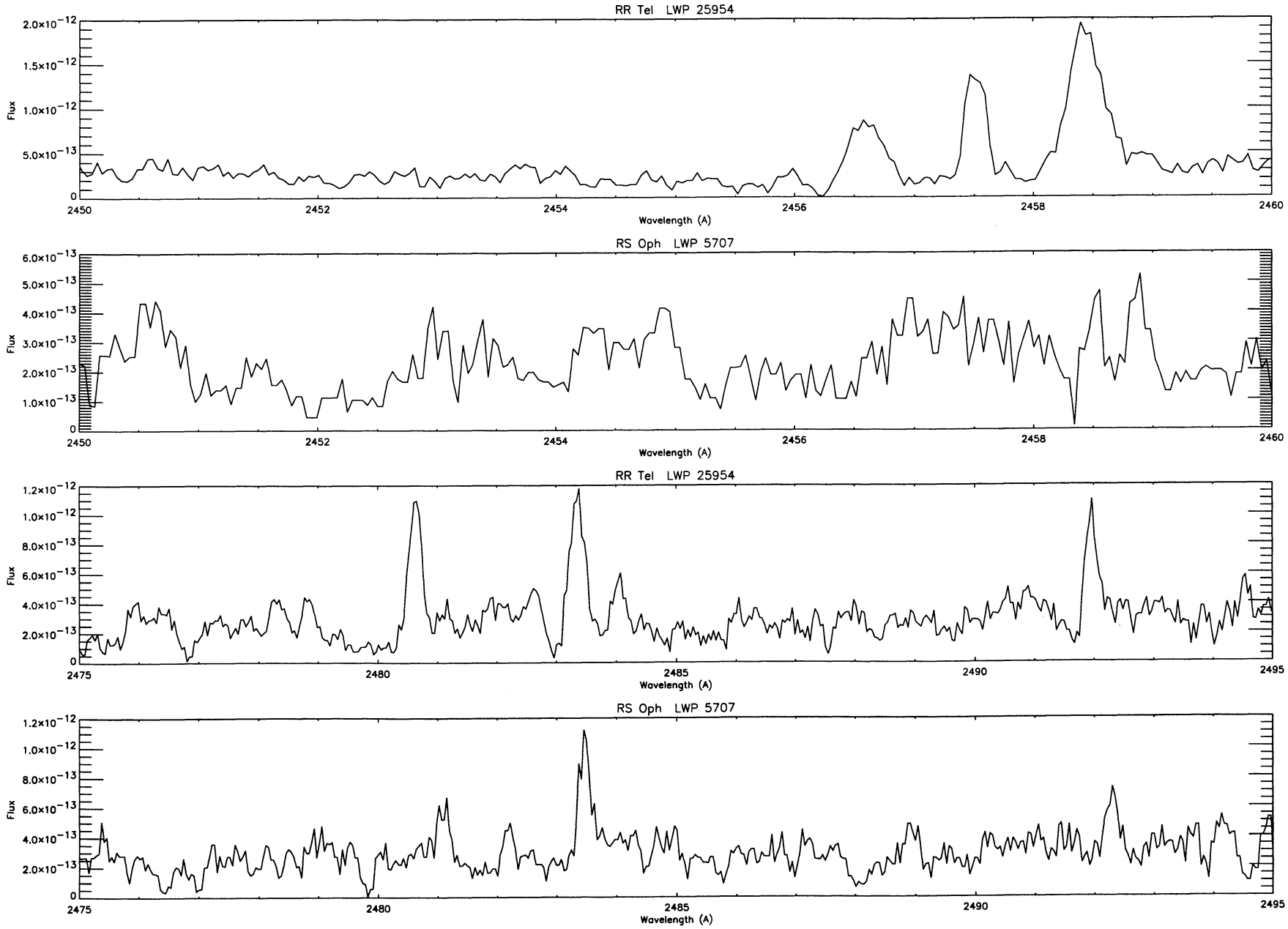

FIG. 6.—Comparison between RR Tel (LWP 25954) and RS Oph (LWP 5707, JD 6164) in two regions showing Fe II fluorescence pumped by the C IV 1550 Å doublet. The fluorescent lines are at 2458, 2481, and 2492 Å. Units are ergs s^{-1} cm^{-2}.

longer sufficient to power the ionization of the wind. A stellar wind appears to have a finite radius for any penetrating shock because of its density gradient. At some stage, the density falls sufficiently that the shock enters free expansion (Ostriker & McKee 1988; Shore 1992). Bode & Kahn (1985) and O'Brian, Bode, & Kahn (1992) have modeled the X-ray emission from RS Oph, assuming that it originated from the expanding ejecta interacting with the stellar wind. From the ultraviolet versus optical variations, we can gain some insight into this process. The time when the narrow emission lines appeared—when they dominated the resonance line profiles and all other emission lines in the ultraviolet—was after JD 2,446,140. The shock effectively exited the wind on this date. The radio light curve (Taylor et al. 1989) peaked on this date and exponentially declined thereafter due to recombination. The same thing happened to the narrow emission lines, and also to the contributors to the visual light curve. Thus the spectral variations support the models that attribute the high-temperature ionizing radiation to shock-generated emission.

The indications are that whatever its origins, the ionizing source turned off very quickly, on a timescale of about 1 month. This is faster than in any other nova yet observed (see Krautter et al. 1995 for discussions of V1974 Cyg 1992). The presence of EUV emission at a late time, as indicated by the detection of the He I 10830 Å infrared line and the O VI Raman line, is consistent with a white dwarf continuum with a color temperature less than 3×10^5 K and does not require strong X-ray emission (see O'Brian et al. 1992). Two factors contribute to this decline in the line strengths, both of which depend on RS Oph's special status as a wind-embedded RN. First, as the gas recombined, the optical depth of the wind increased rapidly. As we will discuss below, the wind column density was of order 10^{21} cm^{-2} during the expansion phase for the ejecta, based on the absorption-line spectrum seen against the broad lines. Thus, as soon as the H II region began to neutralize, the opacity along the line of sight to the remnant increased. However, there must have been a rapid decline in the X-ray output from the central star as well, otherwise the emission from coronal species would not have decayed so fast.

RS Oph must have ejected nearly all its accreted plus mixed core mass, leaving virtually nothing behind to power surface nuclear reactions. A similar case was encountered in V838 Her 1991 (Starrfield et al. 1992; Vanlandingham et al. 1995, in preparation). This suggests a high mass for the white dwarf, quite close to the Chandrasekhar limit, in rough agreement with our derived value for the mass based on the Eddington luminosity. It appears that the hard X-ray emission was derived completely from shocks produced by the expanding ejecta. The ejecta had a kinetic energy of order 9×10^{43} ergs, assuming a mass of $10^{-6}\ M_\odot$ (Borgias et al. 1989; Anupama & Prabhu 1989) and an ejection velocity of 3000 km s^{-1} so that the mean shock X-ray luminosity was $\lesssim 300\ L_\odot$. This is far below the Eddington luminosity for the white dwarf. The high shock speed, however, means that the X-rays emitted from the ejecta were much higher energy than from the remnant. Thus the emission from the ejecta was likely responsible for the ionization of the coronal species.

6. DISCUSSION

6.1. *The Red Giant Wind*

The first indication of the presence of the wind was narrow absorption lines superposed on all of the broad permitted emission lines. The absorption lines are mainly from the iron group species, primarily Fe II and Fe III. Paper I (see Shore et al. 1994a) showed that the pre-UV maximum spectra can be modeled by assuming that there is cool (approximately 5000 K), reasonably opaque gas intervening between us and the white dwarf with a column density of order 10^{21} cm^{-2} for solar metal abundances. The absorption lines became narrower and disappeared coincidentally with the onset of the narrow emission-line phase. This is additional evidence that the expanding Strömgren sphere from the outburst completely ionized the red giant wind.

Following the decline of the broad line phase, the strongest Fe II emission was from multiplets RMT 62, 63, 129, and 373, all of which lie in the wavelength region between 2700 and 2800 Å. The lines were all narrow and formed by recombination within the wind. These identifications were confirmed using LWP 25954, a recent long-exposure high-resolution spectrum of RR Tel. These lines must have come from the same region that was responsible for O III] 1665 Å, Si III] 1892 Å, and C III] 1908 Å. The lines are quite strong and there is no indication of absorption by the cool gas at these later stages. Several of the stronger permitted transitions, such as Si III 1206 Å are likely absorbed by interstellar gas, so that the narrow line is obscured. There is also strong Al II] 2670 Å emission, again probably from the same parts of the wind where the weak Al III 1854, 1863 Å resonance doublet lines are formed. This is a typical spectrum for a symbiotic nova.

Many of the higher excitation lines found in the later RS Oph high-resolution spectra are missing from the RR Tel spectrum. Specifically, two lines of [Fe XI], 1467 Å and 2648 Å do not appear in this slow nova, indicating that the ionization temperature of the initial UV pulse in RS Oph was considerably higher than the central source normally present in a symbiotic binary (see Kenyon et al. 1995). In addition, the high ionization stages encountered in the symbiotic RNe are probably not attained by slow novae because there are no high speed ejecta to provide sufficiently strong X-ray precursors to power the coronal species.

There is strong evidence that the CNO abundances in the red giant are unusual. The carbon and nitrogen resonance lines provide information about the optical depth of the H II region formed by the precursor and shock-generated X-rays. The N V 1240 Å) doublet showed strong emission in the 1242 Å component as soon as the narrow lines appeared, yet even in the last spectrum the 1238 Å ccomponent was still the weaker one. Evidently, the wind was very opaque in this line, suggesting that the red giant is nitrogen-rich. In contrast, the C IV 1550 Å doublet showed nearly nebular ratios for the 1548 Å to 1550 Å components by the last spectrum (SWP 25961). Neither N V nor C IV appears to be affected by interstellar components. Other emission lines that are likely contaminated with interstellar absorption, such as Si IV 1393, 1402 Å, are detected. The decrease in overlying wind absorption accounts for most of the changes in the line ratios, but there seems to be excess absorption of the N V components that is not observed in other symbiotics. Evans et al. (1988) also remark that the anomalous strengths of the infrared CO absorption bands indicate that the red giant may be oxygen-rich.

The strength of the wind emission features argues that there was no Roche lobe overflow powering the prenova. Unless the wind and stream of such a binary can co-exist, the implication is that mass was supplied to the white dwarf by a wind. The line width (FWHM $\approx$ 90 km s^{-1}) is compatible with a normal

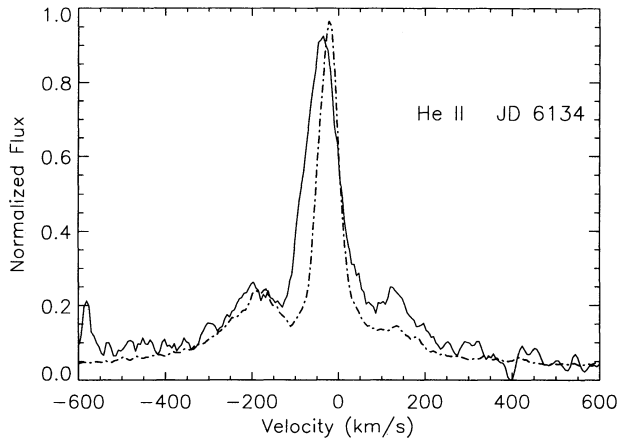

FIG. 7a

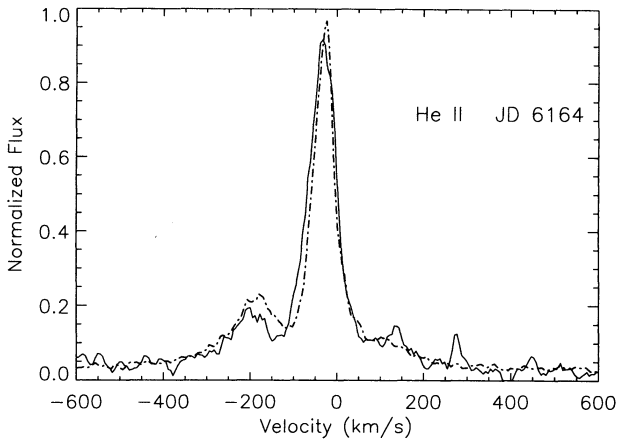

FIG. 7b

FIG. 7.—Comparison between He II 1640 Å (*solid*) and He II 4686 Å (*dashed*) line profiles at two epochs. (*a*) JD 6134, approximately at peak of the integrated line fluxes. (*b*) JD 6164, approximately at shock breakout.

red giant wind. The highest ionization lines are slightly blue-shifted relative to their rest wavelengths, while the permitted resonance lines are usually less shifted. Perhaps we are seeing the effect of the shape of the Strömgren sphere around the nova site.

6.2. *Structure in the Wind Emission Lines*

A broad pedestal, extending from about −220 to +220 km s^{-1}, was present on the narrow lines in the later spectra, as shown in Figures 7 and 8. In addition, there was a separate emission line at high negative radial velocity, whose strength varied with species relative to the central wind component at about 0 km s^{-1} relative velocity. It was relatively strong at −200 km s^{-1} on N IV] 1486 Å, N III] 1750 Å, Si III] 1892 Å, and C III] 1908 Å. It also appeared on [Fe XI] 2648 Å after about JD 2,446,164. Krautter (1986) found similar structure on He I 5876 Å and [Fe X] 6374 Å from 1985 April 10 to 14 (JD 2,446,164–2,446,168), in both cases at −170 km s^{-1}. For He II 4686 Å, the ratio of the strengths of the low to high-velocity features monotonically increased during the later phases of the outburst (Kenyon et al. 1995; see Table 8). He II 1640 Å also showed this feature after JD 2,446,110, before the disappearance of [O I] 1641 Å, but it was gone by JD 2,446,164. This high-velocity component was always weak on the permitted transitions, especially Si IV, C IV, and N V. There was no corresponding emission line at around +200 km s^{-1} on any transition. Figures 7 and 8 show the comparison between line profiles of UV and optical transitions for He II and coronal [Fe IX] and [Fe XIV]. The [Fe VII] 5302 Å coronal line was asymmetric after JD 2,446,150 in the same sense as [Fe XI] 2648 Å and had a strong high-velocity component.

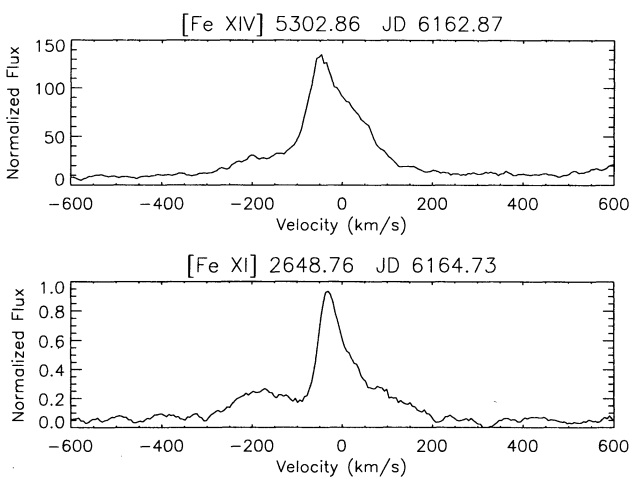

FIG. 8.—Comparison between coronal line profiles. *Top*: [Fe XIV] 5302 Å; *bottom*: [Fe XI] 2648 Å. Note the presence of the high-velocity feature and the asymmetry of the line profiles, the latter being absent on the contemporaneous He II emission lines.

Nussbaumer & Vogel (1989) have modeled line formation and profile development with phase for symbiotic binary winds. They showed that a redshifted asymmetric line should result for any transition coming from the inner portion of the wind at white dwarf inferior conjunction. The blueshifted high-velocity feature cannot be accounted for by their calculations. It appears that there was another geometrically and dynamically distinct feature present in the RS Oph outburst distinguishing it from a normal symbiotic system. We suggest that it is due to postshocked wind material. The emission cannot be from gas immediately behind the shock, since such gas has a velocity approximately $0.75v_{\rm ejecta}$. Downstream of the shock, however, the gas will have cooled and slowed in its expansion.

6.3. *Physical Parameters Derived from Emission-Line Ratios*

As a first estimator of the electron density, we use the Si III] 1892 Å/C III] 1908 Å ratio (see Tables 4 and 7). The integrated line fluxes, obtained from the profiles binned to 0.5 Å, show that the density was about 2×10^{10} cm^{-3} on JD 2,446,123,

TABLE 7

Si III] AND C III] NARROW EMISSION FLUXES[a]

SWP	Si III] High	Si III] Low	C III] High	C III] Low
25328.....	<1.33E−13	8.83E−13	...	4.03E−13
25416.....	1.64E−13	1.18E−12	6.24E−13	8.44E−13
25506.....	3.31E−13	1.34E−12	5.76E−13	6.70E−13
25638.....	3.22E−13	9.26E−13	4.18E−13	4.67E−13
25816.....	5.48E−14	3.12E−13	1.27E−13	2.36E−13
25961.....	...	2.06E−13	<2.34E−13	2.74E−13

NOTE.—All fluxes are in units of ergs s^{-1} cm^{-2}.

[a] The high-velocity feature is at −200 km s^{-1}, the low velocity is at approximately 0 km s^{-1}.

TABLE 8

N V AND C IV NARROW LINE FLUXES

SWP	N V 1238 Å	N V 1242 Å	C IV 1548 Å	C IV 1550 Å
25290.....	...	6.18E−12	...	3.30E−12
25328.....	...	5.23E−12	9.76E−13	4.80E−12
25416.....	1.34E−12	6.48E−12	5.29E−12	4.82E−12
25506.....	1.31E−12	6.29E−12	9.93E−12	5.55E−12
25638.....	1.36E−12	5.33E−12	8.02E−12	5.41E−12
25816.....	5.88E−13	1.39E−12	2.47E−12[a]	1.11E−12[a]
25961.....	<4.4E−13	8.01E−13	1.26E−12	6.89E−13

NOTE.—All fluxes are in units of ergs s^{-1} cm^{-2}.

[a] High-velocity features were measured on the C IV profiles; $F(1548\ Å) = 2.32 \times 10^{-13}$, $F(1550\ Å) = 4.41 \times 10^{-13}$.

which decreased exponentially to about 2×10^9 cm^{-3} by JD 2,446,164. Thereafter, the integrated flux ratio began to increase as the inner portion of the wind contributed progressively more of the line-emission measure. This is shown in Figure 9. We have used the ionization parameter $f = [N(Si^{+2})/N(Si)]/[N(C^{+2})/N(C)] = 0.5$ (Nussbaumer 1986; Nussbaumer & Stencel 1989; Nussbaumer & Storey 1979a, b) for the estimate, although f is likely to be a function of time.

We can separate the narrow emision components by employing the full resolution line profiles. For the low-velocity narrow emission components, this ratio was about 3.0, while for the high-velocity narrow components it was 0.25. The pedestal component had the same Si III]/C III] ratio as the high-velocity component. The derived densities are of order 10^{11} cm^{-3} for the low-velocity component and $\leq 10^9$ cm^{-3} for the high-velocity and pedestal line-forming regions. The variation in the derived electron density is shown in Figure 9*a* and the comparative variations in the densities of the high and low-velocity components on the Si III] and C III] lines are shown in Figure 9*b*.

The N III] 1750 Å multiplet can also be used to measure the electron density over a wide range of electron temperatures (Nussbaumer & Storey 1979a, b; Brage Froese Fischer, & Judge 1995). For SWP 25638, the measured fluxes are listed in Table 9. The low-velocity component yields $n_e \sim 10^{10}$ cm^{-3} from the $F(1754)/F(1752)$ ratio. Unfortunately, the high-velocity component on the 1749.68 Å line is blended with another line in the multiplet, 1748.65 Å but it is possible to separate them in the two spectra near narrow line maximum, SWP 25506 and SWP 25638. They yield $n_e \approx 10^9$ cm^{-3}. The O IV] 1401 Å multiplet also gives consistent values for the electron density in the region of low-velocity line formation of about 10^{10} cm^{-3}, using atomic data from Nussbaumer & Storey (1979a, b), Schild & Nussbaumer (1982), and T. Brage (1995, private communication).

These emission-line fluxes and the derived electron densities indicate that the low-velocity emission was from quiescent gas in the ionized region, while the high-velocity component was coming from shock-heated gas that had cooled. The inner wind dominated the low-velocity emission component, while the outer wind near the breakout radius dominated the pedestal and high-velocity narrow line emitting regions.

6.4. *Models for the Effects of Wind Absorption Lines on the Outburst Spectra*

As discussed in Paper I, the red giant wind surrounding the white dwarf dominates its spectrum, through both the Strömgren sphere and absorption through the iron curtain. Throughout the 1985 outburst, RS Oph was within 0.1 of minimum wind column density for the nova site. Thus changes in the ultraviolet spectrum cannot have been due to orbital modulation. However, since the outburst strongly altered the ionization structure of this environment, we should be able to exploit some of the methods developed in Paper I to analyze changes observed in the UV spectra, since this wavelength region is most strongly contaminated by the absorption from the cool gas and emission from the ionized wind.

We have, therefore, constructed a simple two-component model for the ejecta and H II region. Our aim is to gain further insight into the passage of the ejecta through the wind, and the changes in the ionization produced by the expanding H II region from the flash and the hot remnant. To illustrate a specific case, we display in Figure 10 the sequence for the C IV doublet. The model consists of a broad-line component, with a velocity width (FWHM) of 1000 km s^{-1} and narrow components in the appropriate optically thin ratio. The absorption coefficients were computed using the same slab model routines described in Paper I with $n_e = 10^9$ cm^{-3}, $T_e = 5000$ K, and solar abundances. There were three free parameters: (1) the ratio of the narrow to broad-line emissivity; (2) the absorption column density toward the broad-line region; and (3) the ratio of that column density to the one toward the narrow-line region. In Figure 11 we show the full spectral sequence for C IV during the outburst. The observed C IV 1548 Å to 1550 Å ratio, which was zero at the first appearance of the narrow emission phase, gradually increased to about 2.0 by the end of the spectral sequence.

In order to reproduce the evolution of the C IV profiles, we require that the column density of the cool gas decreases toward both the narrow and broad-line emitting regions. This accounts for the increase in the doublet ratio from zero to the nebular value. In addition, the emission measure of the Strömgren sphere must grow relative to the ejecta. This is required because of the decrease in the broad-line component. Finally,

TABLE 9

N III] AND O IV] NARROW LINE FLUXES

Species	Wavelength (Å)	F(SWP 25638)	F(SWP 25861)	F(SWP 25961)
O IV].....	1401	3.86E−13	3.25E−13	1.20E−13
	1404	1.60E−13	1.44E−13	8.87E−14
	1407	3.12E−14	≤5E−14	<4E−14
N III].....	1746	<5E−14	...	...
	1748	2.34E−12	3.03E−13	3.76E−14:
	1749	2.07E−12	5.38E−13	1.21E−13
	1752	4.07E−13	≤8.5E−14	6.79E−14
	1754	5.73E−13	1.46E−13	...

NOTE.—All fluxes are in units of ergs s^{-1} cm^{-2}.

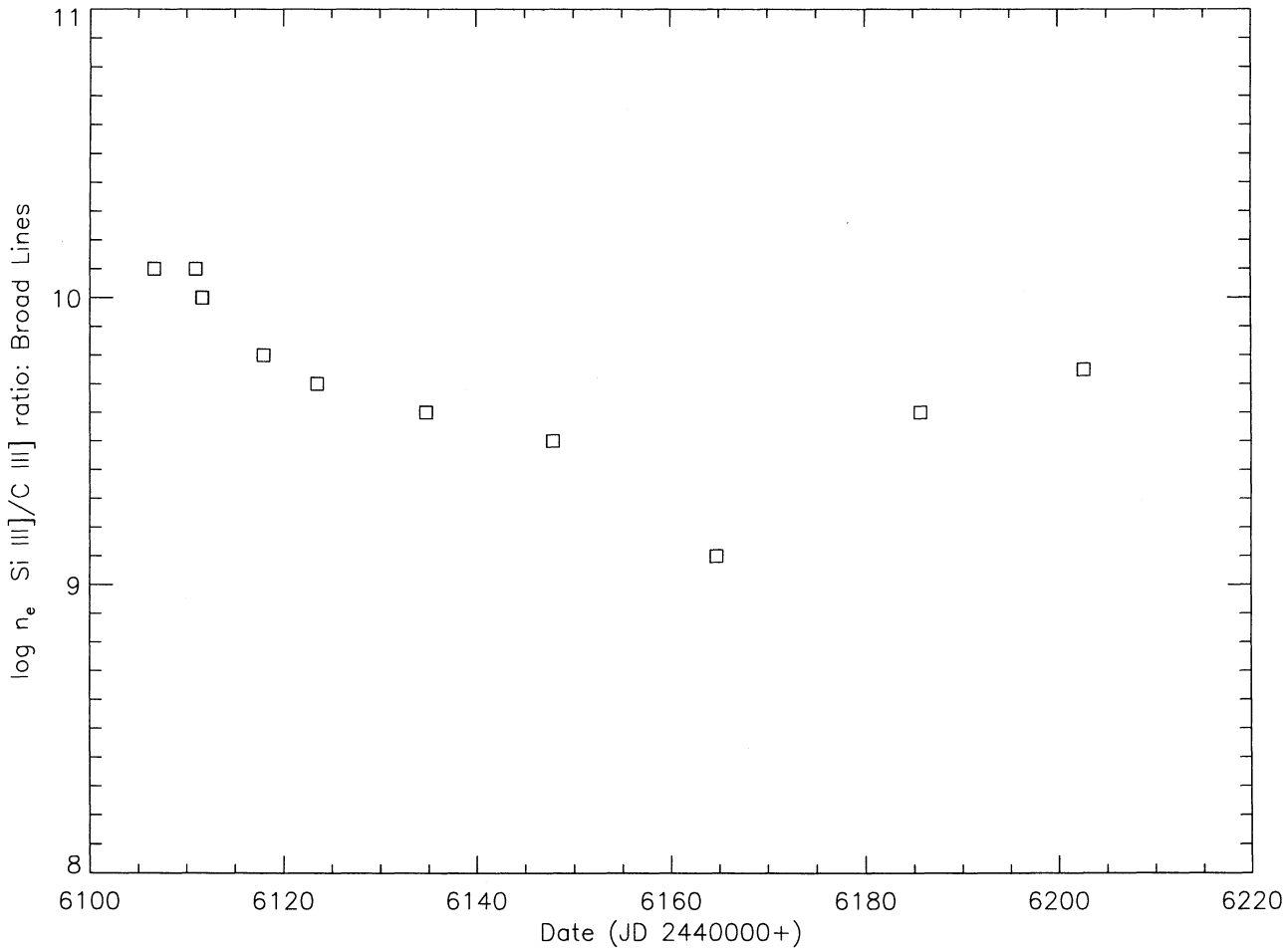

FIG. 9*a*

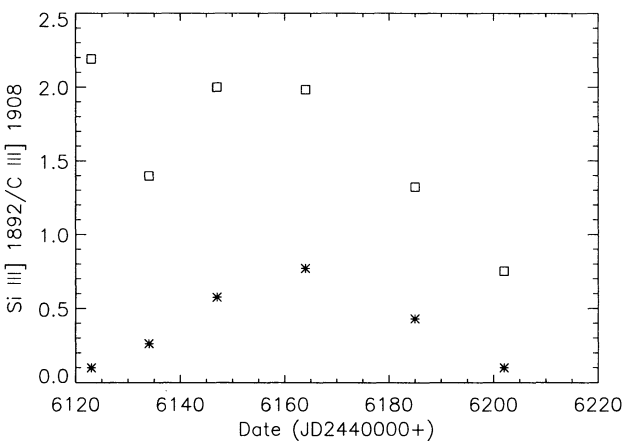

FIG. 9*b*

FIG. 9.—(*a*) Variation in the electron density, n_e derived from the Si III] and C III] integrated fluxes. (*b*) Variation in the Si III]/C III] ratio for the low-velocity (*stars*) and high-velocity (*squares*) components.

after breakout, the decrease in the doublet strength at constant line ratio is what we expect for a recombining gas for which the overlying absorption line contamination has been removed by ionization.

Of course, a full radiative transfer model is required to determine the ionization structure and precise line formation conditions. We feel, however, that the ability of these amazingly simple models to reproduce the observed phenomenology is very encouraging. Perhaps most important it shows that the changes observed in C IV and other resonance multiplets during the earliest stages of the outburst need not be attributed to self-absorption effects. Rather, for Si IV, C IV, and possibly N V, there is strong evidence that the H II region is always optically thin and simply varying in foreground absorption from the cool intervening wind material.

A demonstration of this latter point is shown in Figure 12. Here we plot the normalized strength of the narrow components of C IV against the doublet ratio, $F(1548\ \text{Å})/F(1550\ \text{Å})$. The locus of the observations in this diagram, as a function of time, is the same as the prediction for a variable curtain *without* a change in the emission measure for the C IV region in the wind until JD 2,446,164. The emission decreased thereafter, without a change in the doublet ratio. Because of the complications of the 1400 Å region, a second comparison with model predictions is not possible. Figure 13 shows the derived column densities using the calibration in Paper I. A least-squares fit to the observations shows that the column density in the low-ionization wind decreased over a timescale of about 10 days:

$$N(\text{H}) \approx 9 \times 10^{22}\ \text{cm}^{-2} e^{-(t-t_0)/10}\ ,$$

where t_0 = JD 2,446,118.10. It appears that the H II region in

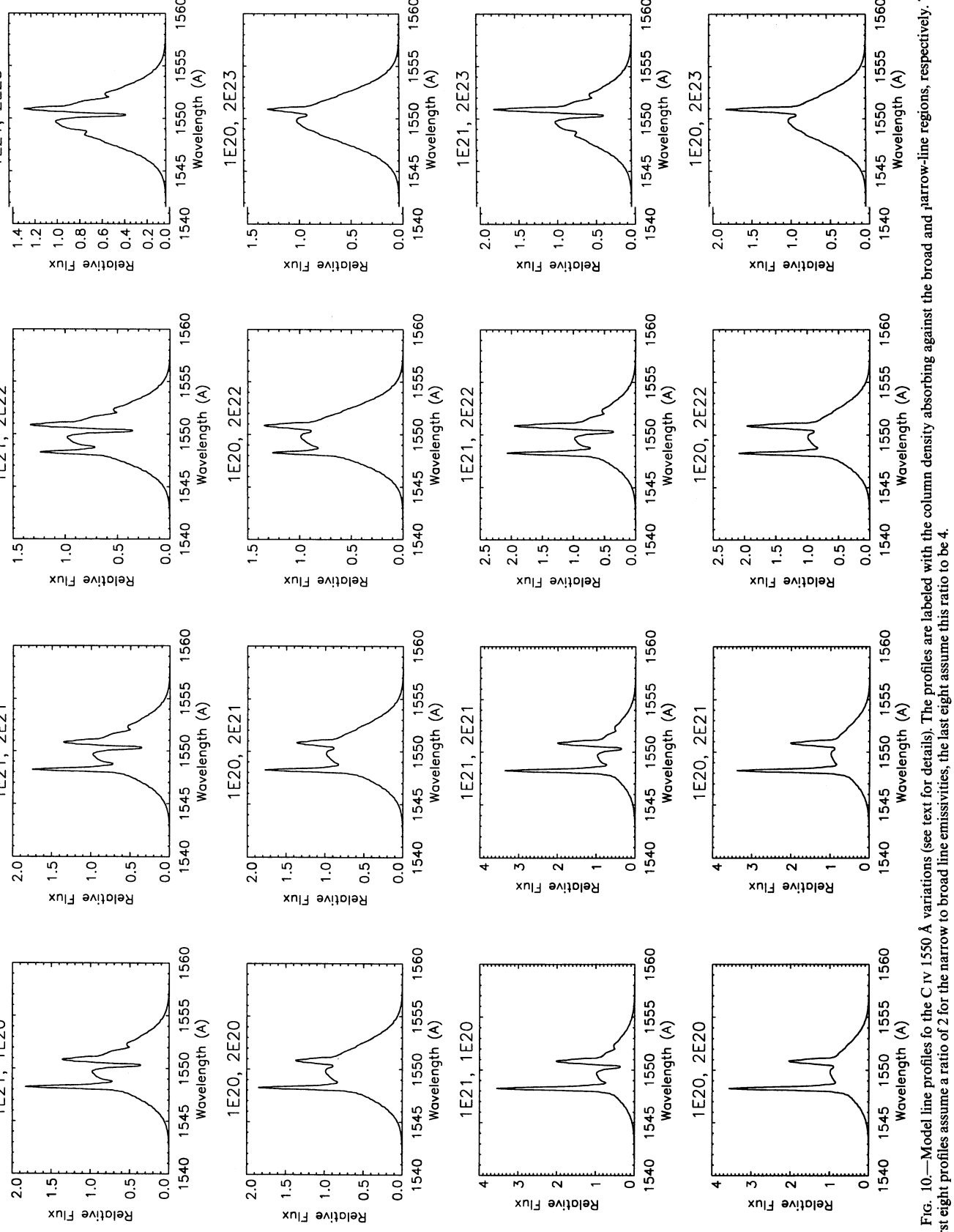

FIG. 10.—Model line profiles fo the C IV 1550 Å variations (see text for details). The profiles are labeled with the column density absorbing against the broad and narrow-line regions, respectively. The first eight profiles assume a ratio of 2 for the narrow to broad line emissivities, the last eight assume this ratio to be 4.

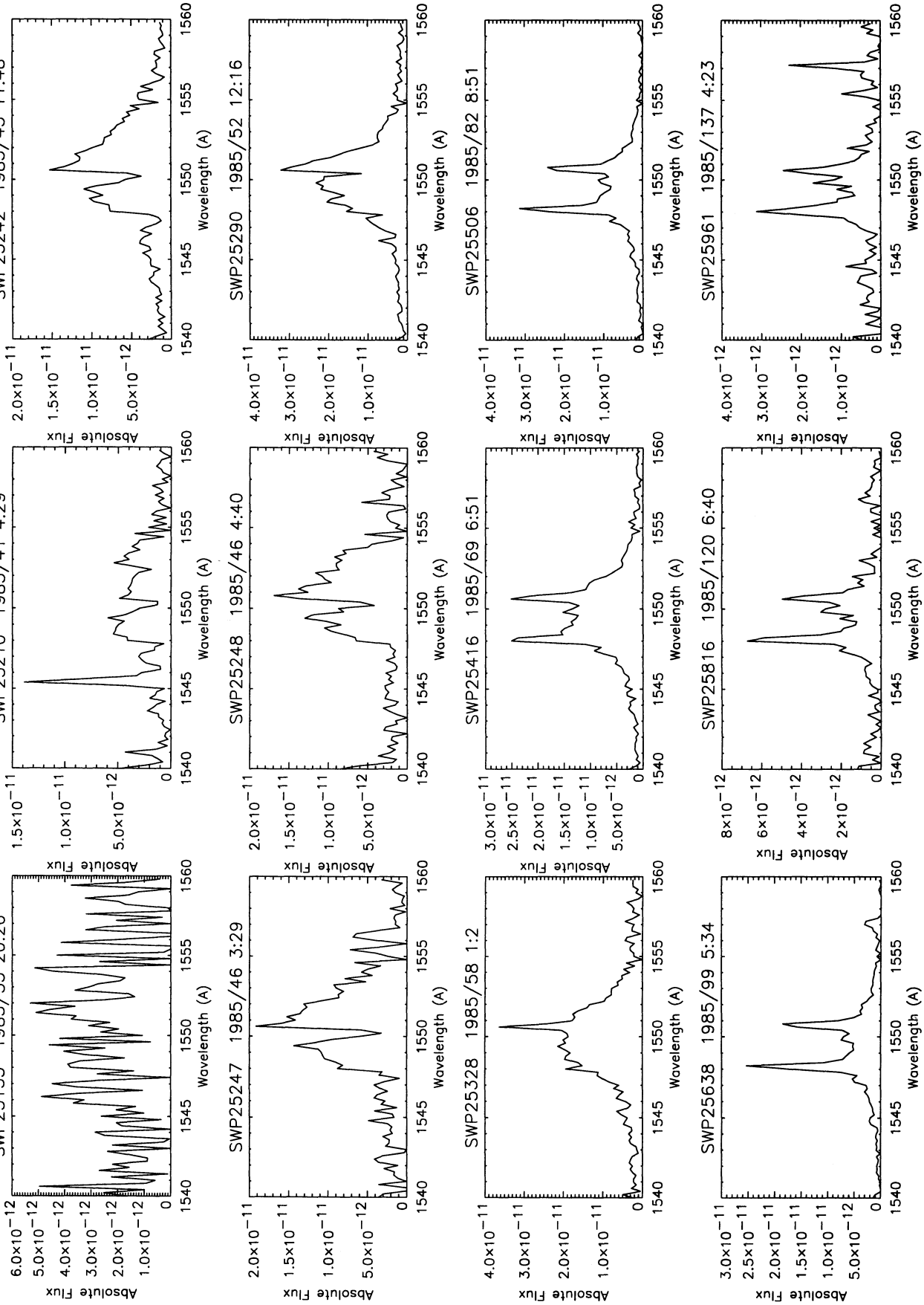

FIG. 11.—Observed variations of C IV 1550 Å for comparison with Fig. 10

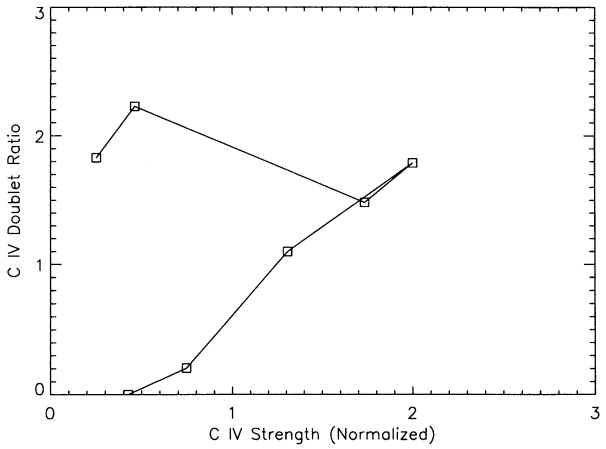

FIG. 12.—Variation of the C IV 1550 Å doublet ratio for comparison with Fig. 10 in Paper I. Note the decrease in doublet strength at constant doublet ratio near the end of this sequence, indicating the onset of recombination of the ionized portion of the wind.

the red giant wind had reached a large radius by JD 2,446,202, the date of the last spectrum. This is approximately the expansion law that would be expected for a (roughly) constant density Strömgren sphere with a constant illuminating source (see also Mürsert & Nussbaumer 1994). This does not mean that the linear size of the emission region was shrinking. Rather, it implies that the ionization of the wind increased rapidly with time as the UV pulse expanded within the envelope and that further ionization of the wind after breakout was powered for a short time by EUV emission from the hot white dwarf.

The weakening of the C IV narrow line emission at constant doublet ratio, due to recombination after JD 2,446,164, agrees with the onset of high-excitation Fe II *emission* in the region longward of 2400 Å by JD 2,446,164. This suggests that recombination had already started soon after the appearance of the narrow-line phase, consistent with a relatively high density in the wind. The final decrease in the C IV doublet strength at constant doublet ratio indicates that the ionization source had turned off and that the envelope was recombining by JD 2,446,185. This agrees very well with the radio observations

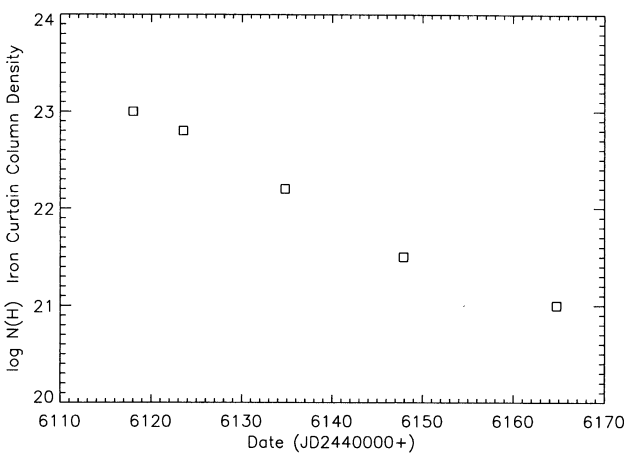

FIG. 13.—(*a*) Variation in the column density, N(H), of the neutral red giant wind derived from the evolution of the narrow C IV components shown in Fig. 12 using the calibration from Paper I (see text for discussion).

which showed that the 2 cm flux had peaked and was decreasing (Spoelstra et al. 1987). Subsequent failures to detect RS Oph in sensitive 2 cm radio surveys of symbiotics indicates that the wind is now largely neutral (Seaquist, Krogulec, & Taylor 1993). The decrease in the thermal radio flux implies a number density of approximately 10^7 cm^{-3}, which supports our estimates obtained from modeling the narrow wind absorption lines.

The continued emission from He I 10830 Å and the infrared Paschen series (Evans et al. 1988) and the slow decay of the ultraviolet O III Bowen fluorescence lines demonstrates that a hot source continued to exist long after the ccoronal line decline had commenced. The high column density we derive implies a substantial soft X-ray opacity which would certainly have precluded directly observing X-ray emission from the white dwarf. The X-ray emission observed by *EXOSAT* must consequently have originated at the expanding shock front, as emphasized by Bode & Kahn (1985), O'Brian & Kahn (1987), and O'Brian et al. (1992). The rapid decrease in coronal line emission indicates that the temperature of the white dwarf was below 10^6 K.

6.5. *Mass-Loss Rate for the Red Giant*

The column density determination provides another important piece of information, the mass-loss rate for the red giant wind. The column density at maximum absorption against the ejecta was about 10^{23} cm^{-2}, which translates to $\dot{M} = 4\pi N(\mathrm{H}) m_p R v \approx 10^{-5}\ M_\odot\ \mathrm{yr}^{-1}$ assuming a wind velocity of 90 km s^{-1} and a radius at breakout of 10^{15} cm. Using the number density obtained from the narrow emission-line analysis above, we find again that $\dot{M} \approx 10^{-5}\ M_\odot\ \mathrm{yr}^{-1}$ for $n_e \approx 10^9$ cm^{-3}. If the ejecta represent the complete removal of the accreted mass, then $\dot{M}_{\mathrm{accretion}} \approx 5 \times 10^{-8}\ M_\odot\ \mathrm{yr}^{-1}$, which is the value that Weight et al. (1994) adopt for the red giant mass-loss rate. They state that this is compatible with the expected wind mass loss for an M2 III star (see also Judge & Stencel 1991, and references therein). However, our results are that the mass-loss rate for the giant was much higher than this at the time of the outburst, perhaps indicating some tidal enhancement of mass loss.

6.6. *Applications to Active Galactic Nuclei*

Our aim in this paper has been to apply the techniques developed for the analysis of symbiotic star winds to a highly time-dependent object, a nova in outburst. The size scale of the system, however, should not deter those working on extragalactic problems from taking an interest in the problem. It is most interesting to note that RS Oph showed many of the characteristics of an active galactic nucleus (AGN) spectrum (e.g., Osterbrock 1989; Malkin, Alloin, & Shore 1989). Its broad-line stage was quickly followed by the kind of composite profile normally associated with Seyfert galaxies. As we have discussed, this is not surprising, since the densities in the different components were quite similar to those derived for such galaxies (Osterbrock 1989). The white dwarf in RS Oph is likely now surrounded by a small accretion disk (compare with discussion in Paper I). It is embedded in a fairly dense gas, but the mass and column densities are comparable to those derived for AGNs, especially Seyfert galaxies (Viegas-Aldovandi & Contini 1989). The wind is not dusty, but D-type symbiotics do contain dust (Kenyon 1986). The progress of the ionization and the ejected mass through the wind mimics many of the phenomena seen in AGNs. In particular, near breakout the spectrum

of RS Oph resembled many Seyfert galaxies. This is not to say that the same dynamical process is responsible for the formation of the spectra of these two very disparate classes of objects. Although the ejecta were axisymmetric (see Bode 1986 and references therein) as seen in many AGNs, there are important differences. We assert, however, that the radiative processes are quite similar and that the RS Oph 1985 outburst can inform the study of active galaxies. Consequently, we recommend this system to the attention of those whose interests lie primarily at large redshift as a model environment against which to test radiative transfer codes and theoretical reconstructions.

7. SUMMARY

We have analyzed the development of the ejecta and circumstellar wind during the 1985 outburst of the long-period symbiotic RN RS Oph. Here we summarize some of our chief results.

We find that the interoutburst UV spectra do not show any evidence for eclipses and support the low-inclination orbital solution obtained from optical spectra. During quiescence, the system appears much like T CrB, although the red giant wind produces a more substantial absorption against the white dwarf in RS Oph. We also find that the evolution of the ultraviolet, optical, and infrared photometry during outburst indicates that the bolometric luminosity of the nova reached the Eddington luminosity of at least a 1.2 $M_\odot$ white dwarf.

Our analysis of the high-resolution optical and UV data show that there were two principal components in the line profiles, whose relative contributions were time-dependent. One was the broad-line component, for which we find that its profile evolution was consistent with a self-similar fluid flow. Consequently, this component of the emission behaved as would be expected from an explosive mass ejection and was inconsistent with mass loss by an episodic accretion event. The other component was the narrow emission lines formed in the ionized region ib the red giant wind.

We find that the ejecta and the initial UV pulse were the principal sources of ionizing radiation. The properties we derive for this ionizing radiation agree with shock models that have been constructed to explain the radio observations. The broad lines were initially dominated by absorption from cool, neutral, or weakly ionized wind gas. As the narrow emission lines appeared, these absorption components vanished. We computed models for the C IV doublet line profile evolution using the techniques developed in Paper I. From these, we show that the column density of the cool material decreased exponentially with time from about 10^{23} cm^{-2} to about 10^{21} cm^{-2} over the first hundred days after outburst with a timescale of about 10 days. At the same time, we show that the emission measure increased for the ionized portion of the wind, manifested in the increase in the strength of the narrow wind emission lines. The models fail, however, to reproduce the behavior of the narrow-line components of N V, although they work well for C IV and He II. This suggests that the nitrogen abundance may be enhanced in the red giant wind.

We further find that the optical and ultraviolet coronal line emission was powered by X-ray emission from the ejecta as they shocked the red giant wind. The decrease in their intensity coincided with the drop in *EXOSAT* X-ray flux, a phase we call shock breakout. Shock breakout was also coincident with a rapid decline in thermal and nonthermal radio emission, and the disappearance of the UV and optical coronal lines. There appear to be two regions contributing to the narrow emission-line formation. One is the expanding H II region within the wind, and the other is a high-velocity region that likely represents cooling post-shocked gas.

We have used the narrow-line flux ratios to derive properties for the wind. We find that Fe II emission and a decrease in the narrow-line C IV doublet emission indicates that recombination occurred soon after shock breakout, and that the density of the line-forming region was quite high, of order 10^9 cm^{-3}, in agreement with the diagnostics drawn from the resonance multiplets in the ultraviolet. The mass-loss rate for the red giant appears to be quite high, about 10^{-5} $M_\odot$ yr^{-1}. Finally, we discussed possible applications of the analysis methods applied to RS Oph 1985 to AGNs. Many of the spectral phenomena seen in this recurrent nova are similar to those encountered in the spectra of Seyfert galaxies. RS Oph presents a unique time-dependent case for the study of the radiative and dynamical interaction of a nova with a dense circumstellar environment.

We thank Jason Aufdenberg, Tomas Brage, Walter Feibelman, Rosario Gonzalez-Riestra, Bob Gehrz, Tom Harrison, Peter Hauschildt, Mario Livio, Janet Mattei, Andy Michalitsianos, Joanna Mikolajewska, Urs Mürset, Harry Nussbaumer, Werner Schmutz, Jim Truran, Manfred Vogel, and Charlie Wu for discussions, Lys Ann Shore for careful reading of the manuscript and Scott Snell for help in obtaining the FES magnitudes. The archival *IUE* data were obtained at GSFC and Vilspa under the nova target of opportunity program headed by A. Cassatella and C.-C. Wu, respectively.

REFERENCES

Anupama, G. C., & Prabhu, T. P. 1989, J. Astrophys. & Astron. 10, 237
Aufdenberg, J. P. 1993, ApJS, 87, 337
Bode, M. F., ed. 1986, RS Ophiuchi (1985) and the Recurrent Nova Phenomenon (Utrecht: VNU Science Press)
Bode, M. F., & Kahn, F. D. 1985, MNRAS, 217, 205
Borgias, J., Echevarria, J., Diego, F., & Sarmiento, J. A. 1989, MNRAS, 238, 1395
Brage, T., Froese Fischer, C., & Judge, P. G. 1995, ApJ, in press
Cassatella, A., Hassall, B. J. M., Harris, A., & Snijders, M. A. J. 1985, in Recent Results on Cataclysmic Variables (ESA SP-236), 281
Dobrzycka, D., & Kenyon, S. J. 1994, AJ, 108, 2259
Doschek, G. A., & Feibelman, W. A. 1993, ApJS, 87, 331
Evans, A., Callus, C. M., Albinson, J. S., Whitelock, P. A., Glass, I. S., Carter, B., & Roberts, G. 1988, MNRAS, 234, 755
Fawcett, B. C. 1988, Atom. Data Nucl. Data Tables, 40, 1
Gonzalez-Riestra, R. 1992, A&A, 265, 71
Hanes, D. A. 1985, MNRAS, 213, 443
Hauschildt, P. H., Starrfield, S., Austin, S., Wagner, R. M., Shore, S. N., & Sonneborn, G. 1994, ApJ, 422, 831
Hauschildt, P. H., Starrfield, S., Shore, S. N., Allard, F., & Baron, E. 1995, ApJ, in press
Hauschildt, P. H., Wehrse, R., Starrfield, S., & Shaviv, G. 1992, ApJ, 393, 307
Hjellming, R. M., van Gorkom, J. H., Seaqwuist, E. A., Taylor, A. R., Padin, S., Davis, R. J., & Bode, M. F. 1986, ApJ, 305, L71
IUEDAC Staff *IUE Observatory*, 1994, *IUE* Data Analysis Center User's Tutorial Manual (Green Belt: Goddard Space Flight Center)
Iijima, T., Strafella, F., Sabbadin, F., & Bianchini, A. 1994, A&A, 283, 919
Itoh, H., & Hachisu, I. 1990, ApJ, 358, 551
Johansson, S. 1983, MNRAS, 205, 71P
Judge, P. & Stencel, R. 1991, ApJ, 371, 357

Kenyon, S. J. 1986, The Symbiotic Stars (Cambridge: Cambridge Univ. Press)
Kenyon, S. J., McCrosky, R. E., Shore, S. N., & Aufdenberg, J. P. 1995, ApJS, in preparation
Krautter, J. 1986, in RS Ophiuchi (1985) and the Recurrent Nova Phenomenon ed. M. F. Bode (Utrecht: VNU Science Press), 23
Krautter, J., Ögelman, H., Starrfield, S., Wichmann, R., & Trümper, J. 1995, ApJ, submitted
Latham, D. W. 1985, in Stellar Radial Velocities, IAU Colloquium No. 88, ed. A. G. D. Philip & D. W. Latham (Schenectady: Davis), 21
Livio, M., Truran, J. W., & Webbink, R. F. 1986, ApJ, 308, 736
Loomis, C. 1994, IUE Newsletter No. 54, 29
Malkin, M. A., Aloin, D., & Shore, S. N. 1989, in Exploring the Universe with the *IUE* Satellite, ed. Y. Kondo (Dordrecht: Kluwer), 655
Mason, K. O., Cordova, F. A., Bode, M. F., & Barr, P. 1986, in RS Ophiuchi (1985) and the Recurrent Nova Phenomenon ed. M. F. Bode (Utrecht: VNU Science Press), 167
Meier, S. R., Kafatos, M., Fahey, R. P., & Michalitsianos, A. G. 1994, ApJS, 94, 183
Mürset, U., & Nussbaumer, H. 1994, A&A, 282, 587
Nussbaumer, H. 1986, A&A, 155, 205
Nussbaumer, H., & Stencel, R. E. 1989, in Exploring the Universe with the *IUE* Satellite, ed. Y. Kondo (Dordrecht: Kluwer), 203
Nussbaumer, H., & Storey, P. J. 1979a, A&A, 71, L5
———. 1979b, A&A, 75, L17
———. 1982, A&A, 115, 205
Nussbaumer, H., & Vogel, M. 1989, A&A, 182, 51
O'Brian, T. O., Bode, M. F., & Kahn, F. D. 1992, MNRAS, 255, 683
O'Brian, T. O., & Kahn, F. D. 1987, MNRAS, 228, 277
Osterbrock, D. 1989, Astrophysics of Gaseous Nebulae and Active Galactic Nuclei (Sacramento: University Science Books)
Ostriker, J. P., & McKee, C. 1988, Rev. Mod. Phys., 60, 1
Payne-Gaposchkin, C. 1957, The Galactic Novae (New York: Dover)
Rosino, L. 1986, in RS Ophiuchi (1985) and the Recurrent Nova Phenomenon ed. M. F. Bode (Utrecht: VNU Science Press), 1
Rosino, L., & Iijima, T. 1986, in RS Ophiuchi (1985) and the Recurrent Nova Phenomenon, M. F. Bode (Utrecht: VNU Science Press), 27
Schild, H., & Nussbaumer, H. 1982, A&A, 124, 279
Schmid, H. M. 1989, A&A, 211, L31
Seaquist, E. R., Krogulec, M. K., & Taylor, A. R. 1993, ApJ, 410, 260
Shore, S. N. 1992, An Introduction to Astrophysical Hydrodynamics (San Diego: Academic)
Shore, S. N., & Aufdenberg, J. P. 1993, ApJ, 416, 355 (Paper I)
Shore, S. N., Livio, M., & van den Heuvel, E. P. J. 1994a, Interacting Binaries: Saas-Fee Advanced Course 22 ed. H. Nussbaumer & A. Orr (Berlin: Springer)
Shore, S. N., Sonneborn, G., & Starrfield, S. 1990, in Evolution in Astrophysics: *IUE* Astronomy in the Era of New Space Missions (ESA SP-310), 447
Shore, S. N., Sonneborn, G., Starrfield, S., Gonzalez-Riestra, R., & Polidan, R. S. 1994b, ApJ, 421, 344
Shore, S. N., Starrfield, S., Sonneborn, G., Gonzalez-Riestra, R., & Ake, T. B., III 1993, AJ, 106, 2408
Shore, S. N., Starrfield, S., Sonneborn, G., Williams, R. E., Haumy, M., Cassatella, A., & Drechsel, H. 1991, ApJ, 370, 193
Snijders, M. A. J. 1986, in RS Ophiuchi (1985) and the Recurrent Nova Phenomenon ed. M. F. Bode (Utrecht: VNU Science Press), 51
Snijders, M. A. J. 1987, Ap&SS, 130, 243
Spoelstra, T. A. T., Taylor, A. R., Pooley, G. G., Evans, A., & Abinson, J. S. 1987, MNRAS, 224, 791
Starrfield, S., Sparks, W. M., & Truran, J. W. 1974, ApJS, 28, 247
Starrfield, S. 1989, in The Classical Novae ed. M. Bode & A. Evans (NY: Wiley), 39
Starrfield, S. 1993, in The Realm of Interacting Binaries ed. J. Sahade, G. M. McClusky, & Y. Kondo (Dordrecht: Kluwer), 209
Starrfield S., & Snijders, M. A. J. 1987, in Exploring the Universe with the *IUE* Satellite ed. Y. Kondo (Dordrecht: Kluwer), 377
Starrfield, S., Sparks, W. M., & Shaviv, G. 1988, ApJ, 325, L35
Starrfield, S., Sparks, W. M., & Truran, J. W. 1985, ApJ, 291, 136
Starrfield, S., Shore, S. N., Sparks, W. M., Sonneborn, G., Truran, J. W., & Politano, M. 1992, ApJ, 391, L71
Taylor, A. R., Davis, R. J., Porcas, R. W., & Bode, M. F. 1989, MNRAS, 237, 81
Vanlandingham, K., et al. 1995, in preparation
Viegas-Aldovandi, S. M., & Contini, M. 1989, A&A, 215, 253
Weight, A.. Evans, A., Naylor, T., Wood, J. H., & Bode, M. F. 1994, MNRAS, 266, 761
Williams, R. E., Sparks, W. M., Gallagher, J. S., III, Ney, E. P., Starrfield, S., & Truran, J. W. 1981, ApJ, 251, 221